JOC The Journal of Organic Chemistry

pubs.acs.org/joc Article

Nucleoside Analogues with a Seven-Membered Sugar Ring: Synthesis and Structural Compatibility in DNA−RNA Hybrids

Sunit Kumar Jana, S. Harikrishna, Sruthi Sudhakar, Roberto El-Khoury, P.I. Pradeepkumar,* and Masad J. Damha*

Cite This: J. Org. Chem. 2022, 87, 2367−2379 Read Online

ACCESS | Metrics & More | Article Recommendations | Supporting Information

ABSTRACT: Herein we describe results on the pairing properties of synthetic DNA and RNA oligonucleotides that contain nucleotide analogues with a 7-membered sugar ring (oxepane nucleotides). Specifically, we describe the stereoselective synthesis of a set of three oxepane thymine nucleosides (OxT), their conversion to phosphoramidite derivatives, and their use in solid-phase synthesis to yield chimeric OxT-DNA and OxT-RNA strands. The different regioisomeric OxT phosphoramidites allowed for positional variations of the phosphate bridge and assessment of duplex stability when the oxepane nucleotides were incorporated in dsDNA, dsRNA, and DNA−RNA hybrids. Little to no destabilization was observed when two of the three regioisomeric OxT units were incorporated in the DNA strand of DNA−RNA hybrids, a remarkable result considering the dramatically different structure of oxepanes in comparison to 2′-deoxynucleosides. Extensive molecular modeling and dynamics studies further revealed the various structural features responsible for the tolerance of both OxT modifications in DNA−RNA duplexes, such as base−base stacking and sugar−phosphate H-bond interactions. These studies suggest that oxepane nucleotide analogues may find applications in synthetic biology, where synthetic oligonucleotides can be used to create new tools for biotechnology and medicine.

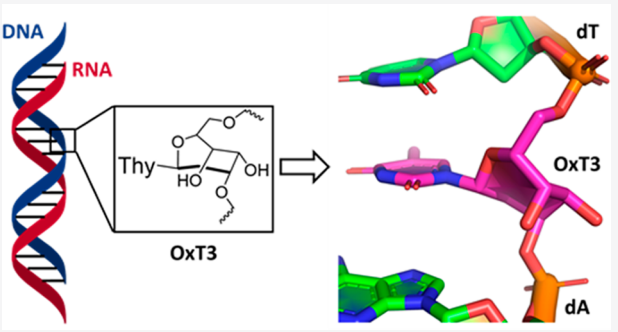

INTRODUCTION

The advent of synthetic biology has warranted investigation into additional nucleoside modifications for the purpose of creating new genetic polymers (XNA) in which the natural nucleosides found in RNA and DNA have been replaced by an unnatural moiety.[1−3] Furthermore, nucleoside analogues have found an increasingly important place in modern drug discovery. They find use as antiviral and anticancer agents, as structural probes for studying nucleic acid/protein interactions, and as precursors of therapeutic oligonucleotides (e.g., antisense, siRNA, crRNA, etc.).[4−6] We previously reported on nucleosides containing a seven-membered sugar (oxepane) ring.[7,8] Elaboration to the phosphoramidite derivatives allowed for the solid-phase synthesis of oxepane nucleic acid (ONA) sequences connected via 5′-7′ linkages (OxT_0, OxA_0; Scheme 1).

Notably, we found that ONA/RNA hybrids were substrates of RNase H and that ONA strands were resistant to hydrolysis by endonucleases in biological media,[7] two important requirements of oligonucleotides being used in antisense and RNAi therapeutic modalities. However, the poor affinity of 5′-7′-ONAs (OxT_0 and OxA_0) toward a complementary RNA target would limit their use in gene silencing approaches that target RNA.[7] Due to this limitation, we adopted two approaches to increase the thermal stability of ONA/RNA duplexes: (i) introduction of additional functional groups in the oxepane ring to steer the sugar conformation that may favor binding to RNA (e.g., OxT_1; Scheme 1) and (ii) moving the location of phosphodiester backbone closer to the nucleobase to better mimic the native DNA or RNA backbone, e.g., 4′-7′ and 3′-7′ linked ONAs (OxT_2 and OxT_3; Scheme 1). The choice of the nucleosides, alone or inside a duplex, is guided by classical molecular dynamics (MD) simulations and quantum mechanical calculations as reported recently by our groups.[8,10−13] Herein, we present the stereoselective functionalization of the unsaturated oxepine nucleosides, their elaboration into phosphoramidite derivatives by careful selection of orthogonal protecting groups, and microwave-assisted phosphitylation of their sterically hindered hydroxyl groups. We also describe the incorporation of oxepane nucleoside units into DNA and RNA strands via solid-phase synthesis and the impact of these modifications on the structure and thermal stability of dsRNA, dsDNA, and RNA−DNA hybrid duplexes.

Received: September 15, 2021
Published: February 8, 2022

Scheme 1. Synthetic Pathways for the Synthesis of Oxepane Nucleic Acids (Past and Present Work)

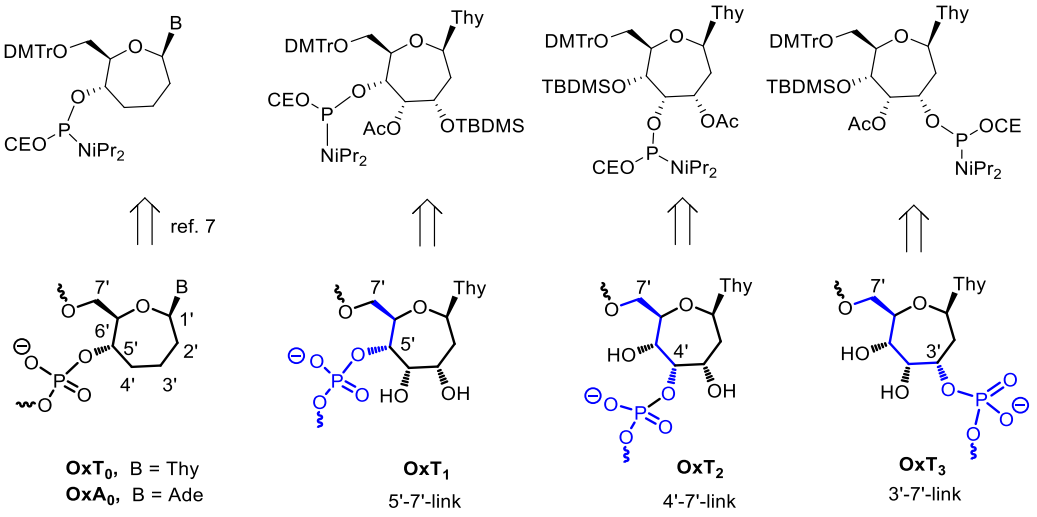

Scheme 2. Synthesis of Phosphoramidite Derivative P_1[a]

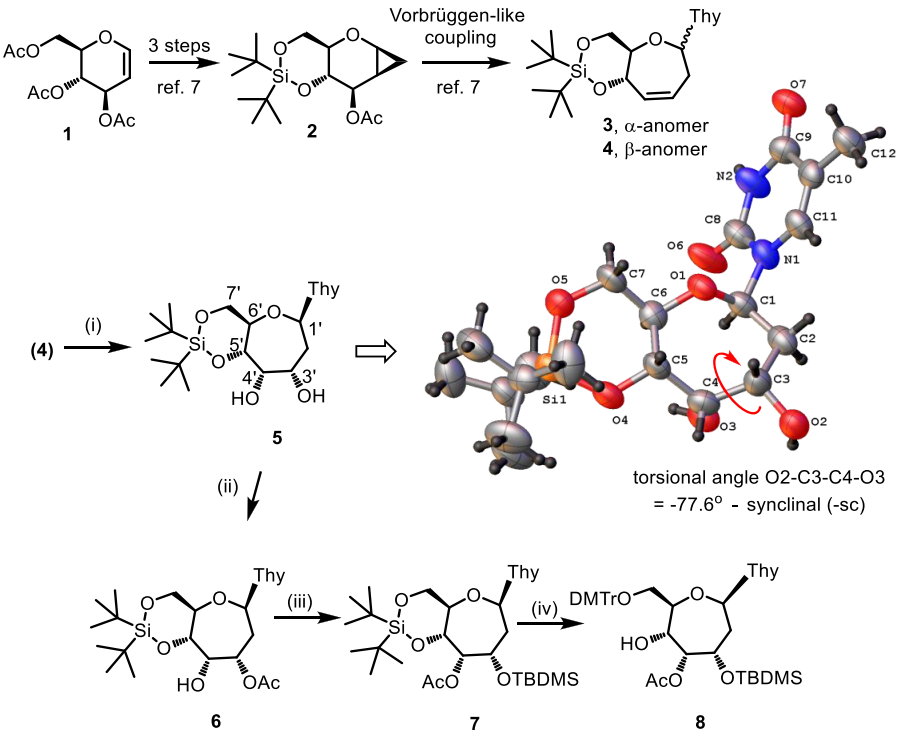

[a]Reagents and conditions: (i) AD-mix-α, *tert*-butyl alcohol and water (1:1, v/v), 0 °C, 16 h, 84%; (ii) Ac_2O, DMAP, pyridine, rt, 1 h, 80%; (iii) TBDMS-Cl, imidazole, pyridine/DMF (1:1, v/v), 120 °C, 16 h, 72%; (iv) (a) pyridine-HF, pyridine/THF (1:1, v/v), 0 °C, 15 min (b) DMTr-Cl, pyridine, rt, 3 h, 54% (over two steps). The crystal structure for compound **5** is shown (CCDC deposition no. 2108264).

RESULTS AND DISCUSSION

Nucleoside Synthesis. First, we aimed to access diastereomerically enriched dihydroxylated oxepane analogue **5** by ring expansion of cyclopropanated glucal **2**[7,9] (prepared from **1**) with silylated thymine to afford oxepine anomers **3** and **4** (Scheme 2).[7] Sharpless asymmetric dihydroxylation (SAD) of **4** with OsO_4 in the presence of a chiral quinine ligand (i.e., AD-mix-α) led to the formation of **5**, with no other diastereomer observed. Classical methods by treatment of **4** with OsO_4 only led to the formation of inseparable diastereomeric dihydroxylated compounds. The structure of **5** was unambiguously confirmed through extensive NMR spectroscopy (^1H, ^{13}C, COSY, HMBC, HSQC, and NOESY) experiments (Supporting Information) and by single-crystal X-ray diffraction (Scheme 2).

Treatment of **5** with 1 equiv of acetic anhydride led to exclusive acylation at the less hindered 3′-hydroxyl group to give **6** in 80% isolated yield. Interestingly, no migration of the 3′-OAc group to the 4′ position occurred when **6** was left standing in pyridine at room temperature or elevated temperatures (40–120 °C). One possible explanation for this observation is the relative disposition of the substituents at C3′/C4′, being in an "anti"-like conformation, a result of the constraints imposed by the fused siloxane ring. Notably, the torsional angle around C3′

https://doi.org/10.1021/acs.joc.1c02254
J. Org. Chem. 2022, 87, 2367−2379

Scheme 3. Reagents and Conditions[a]

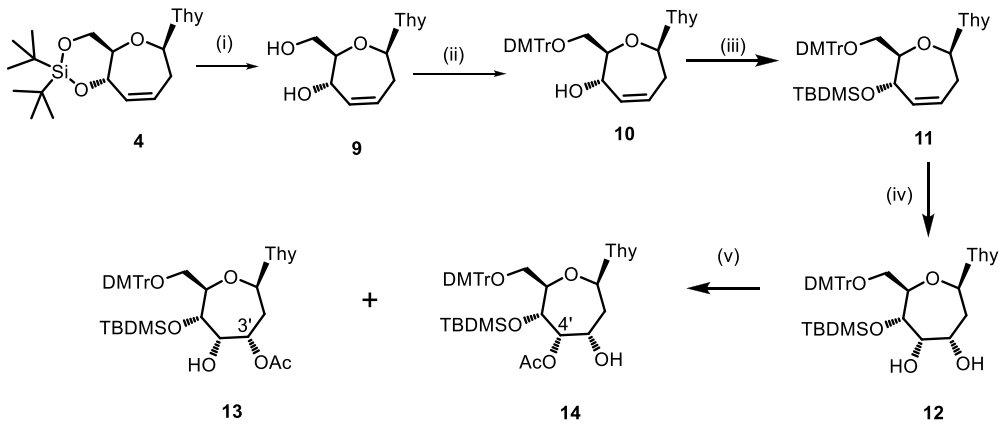

[a](i) (1 M) TBAF in THF, 0 °C, 3 h, 72%; (ii) DMTr-Cl, pyridine, rt, 3 h, 60%; (iii) TBDMS-Cl, imidazole, DMF, rt, 16 h, 94%; (iv) OsO_4 (2.5% in *t*-BuOH), 4-methylmorpholine-4-oxide (NMO), acetone/water (5:1, v/v), 0 °C to rt, 16 h, 80%; (v) Ac_2O, DMAP, pyridine, rt, 1 h, **13** 78%, **14** 8%.

and C4′ in **5** (assumed to be similar in **6**) is −77.5° (Scheme 2), whereas that in native ribonucleosides are about 40−45°.[14]

After successful installation of the 3′-OAc group, we attempted to introduce a *tert*-butyl dimethyl silyl (TBDMS) group at the 4′-position as an orthogonal protecting group (Scheme 2). Treatment of **6** under standard conditions (TBDMS-Cl, imidazole in DMF) failed to produce any significant amount of product, even under harsher reaction conditions (120 °C, 16 h). The same result was observed when **6** was treated with excess benzoyl chloride in pyridine (rt, 16 h), highlighting the steric hindrance of the 4′-OH group. Silylation of **6** occurred efficiently only when pyridine was added as a cosolvent, using a 4-fold excess of TBDMS-Cl/imidazole, and heating the solution at 120 °C for 16 h. Surprisingly, **6** underwent silylation at O3′, with the migration of the acetyl group to O4′, resulting in the formation of nucleoside **7** in a 72% isolated yield. No other product was observed. Full NMR structural characterization of **7** is provided in the Supporting Information. To investigate this phenomenon further, compound **6** was treated with either imidazole in pyridine or with pyridinium chloride in the absence of TBDMS-Cl for 16 h at 120 °C. No acetyl migration was observed under either reaction condition. Thus, the presence of all three components, i.e., pyridine, TBDMS-Cl, and imidazole, and high temperatures are necessary to promote migration of the acetyl group, leading to conversion of **6** to **7**. Treatment of **7** with pyridine-HF at 0 °C for 10 min cleaved the silyl bridge selectively without removing the TBDMS group.[15] This was followed by a reaction with DMTr-Cl in pyridine to provide **8** in 54% yield over the two steps.[15]

To access the regioisomers of compound **8**, oxepane **4** was treated with TBAF to give diol **9** (80% yield), which was then protected by reaction with DMT-Cl/pyridine (**10**; 60% yield) and TBDMS-Cl/imidazole (**11**; 94% yield) (Scheme 3). Treatment of alkene **11** with ADmix-α in *t*-BuOH and water resulted in the formation of **12** as a single diastereomer (40% yield). The yield was improved to 60% upon treatment with ADmix-β and further improved to 80% upon simple treatment with OsO_4 in *t*-BuOH. Gratifyingly, the TBDMS group did not migrate during the dihydroxylation reaction, and the formation of a single diastereomer (**12**) was observed under all of these conditions. Next, diol **12** was reacted with 1 equiv of acetic anhydride to give a separable mixture of **13** and **14** (ca. 10:1 ratio) in 86% combined yield (Scheme 3). The regioselectivity of this reaction is likely controlled by the steric hindrance surrounding the 4′-OH, thus providing more of the 3′-OAc isomer.

Scheme 4. Synthesis of Oxepane Nucleoside Phosphoramidites

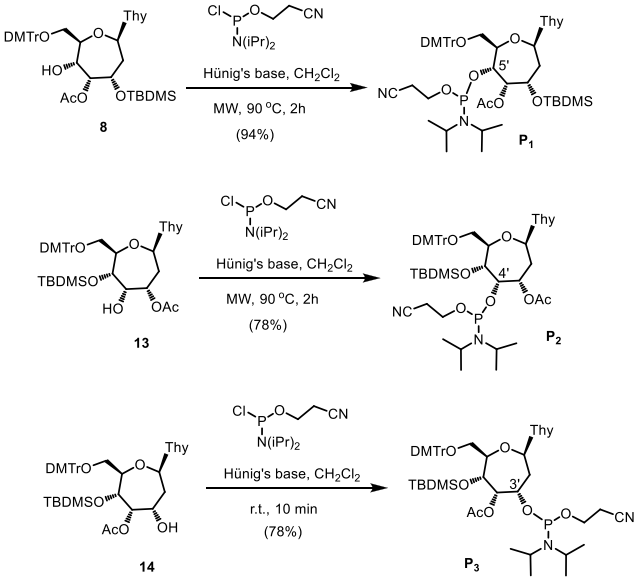

Oxepane Phosphoramidite Synthesis. The synthesized regioisomers **8**, **13**, and **14** represented the immediate precursors to the desired phosphoramidite regioisomers $\mathbf{P_1}$, $\mathbf{P_2}$, and $\mathbf{P_3}$, respectively. To access $\mathbf{P_1}$, nucleoside **8** was phosphitylated under standard protocols with 2-cyanoethyl *N*,*N*,-diisopropylchlorophosphoramidite and Hünig's base (diisopropylethyl amine, DIPEA) using either DCM, THF, dioxane, or dichloroethane as the solvent (see Supporting Information). However, none of these conditions afforded $\mathbf{P_1}$ even after prolonged reaction times. Changing the phosphitylating reagent to 2-cyanoethyl-*N*,*N*,*N*′,*N*′-tetraisopropyl phosphorodiamidite (activated with either tetrazole or 4,5-dicyanoimidazole) made no difference. Finally, microwave-assisted phosphitylation at 90 °C for 2 h with excess 2-

https://doi.org/10.1021/acs.joc.1c02254
J. Org. Chem. 2022, 87, 2367−2379

Scheme 5. (a) Treatment of 8 with NaOMe, Methanol at rt for 10 min Affords a Mixture of Separable Mono Silylated Oxepane Regioisomers; (b) Attempts to Phosphitylate the 4′-TBDMS Isomer at the Less Hindered 3′-OH Led to No Reaction (rt) or a Mixture of Compounds (MW Irradiation)

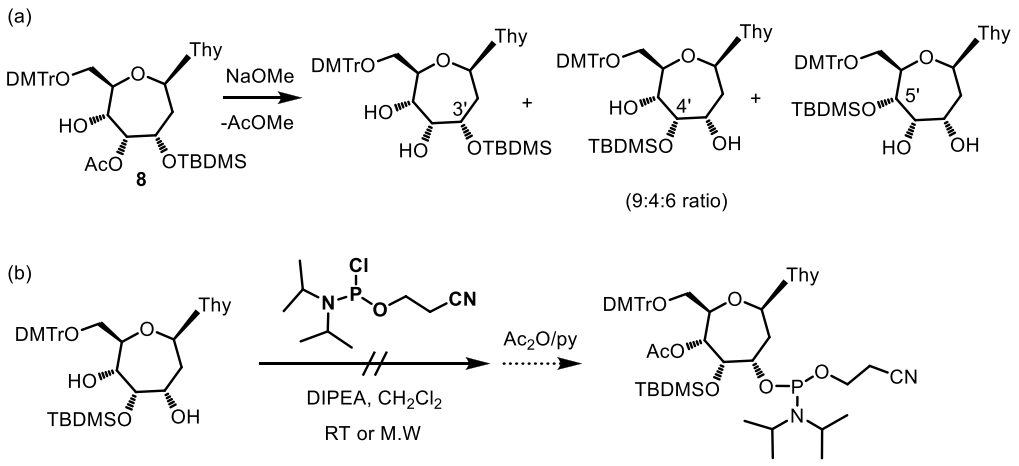

Table 1. T_m Values of Duplexes with Oxepane Modification in the RNA or DNA Strand[a]

		target DNA strand 5′-d(GCTATAATGG)-3′		target RNA strand 5′-r(GCUAUAAUGG)-3′	
modified strand	nucleotide X used in modified strand	T_m (°C)	ΔT_m (°C)	T_m (°C)	ΔT_m (°C)
5′-r(CCAUXAUAGC)-3′	R-rU	31.4		42.8	
	R-OxT$_1$	18.1	−13.3	24.8	−18.0
	R-OxT$_2$	18.3	−13.1	27.3	−15.5
	R-OxT$_3$	18.4	−13.0	30.5	−12.3
5′-d(CCATXATAGC)-3′	D-dT	33.8		31.0	
	D-OxT$_1$	18.1	−15.7	18.2	−12.8
	D-OxT$_2$	29.5	−4.3	30.0	−1.0
	D-OxT$_3$	29.8	−4.0	31.0	0.0

[a] T_m values were measured in 5 mM disodium hydrogen phosphate (Na_2HPO_4) buffer (pH 7.3) containing 140 mM KCl and 1 mM $MgCl_2$ with each strand concentration of 1.5 μM. ΔT_m = (T_m of the modified duplex − T_m of the corresponding unmodified duplex). X indicates the position of rU or modified OxT nucleotide. T_m values were determined as the maximum of the first derivative of the melting curve (A_{260} vs T) and reported as the average of three measurements of the sample. Error analysis of T_m and ΔT_m values are provided in the Supporting Information.

Table 2. Thermodynamic Data of Duplex Formation for Oxepane-Modified DNA Hybridized to Complementary RNA[a]

antisense DNA strand 5′-d(CCATXATAGC)-3′ X	ΔH (kJ/mol)	ΔS (J/K/mol)	ΔG at 300 K (kJ/mol)
D-dT	−196.1 ± 3.3	−537.6 ± 11.0	−34.8 ± 0.1
D-OxT$_1$[b]			
D-OxT$_2$	−258.4 ± 3.7	−746.0 ± 11.7	−34.6 ± 0.2
D-OxT$_3$	−308.3 ± 2.9	−907.0 ± 8.1	−36.1 ± 0.2

[a] Thermodynamic data were calculated from the heating curves presented in Figure 1A. [b] Melting transitions occur at temperatures that are too low, making it difficult to draw lower baselines with high certainty.

cyanoethyl *N,N,*-diisopropylchlorophosphoramidite/DIPEA led to the formation of $\mathbf{P_1}$ in 94% yield (Scheme 4). This highlights the steric hindrance (and poor reactivity) of the 5′-OH group, which can be addressed by microwave irradiation over a 2 h period.[16] These experiments also underline the remarkable thermal stability of $\mathbf{P_1}$.

Phosphitylation of **13** required microwave radiation at 90 °C for 2 h, providing $\mathbf{P_2}$ in 78% yield (Scheme 4). By contrast, a reaction at an ambient temperature (no MW) for 10 min afforded $\mathbf{P_3}$ from **14** in 78% yield (Scheme 3). The drastic differences in reaction conditions highlight the different reactivities of the 4′/5′ vs 3′-OH groups.

We also considered **8** as a precursor to the other oxepane phosphoramidite derivatives (Scheme 5). For example, treatment of **8** under basic conditions resulted in a mixture of 3′, 4′, and 5′-TBDMS isomers (9:4:6 ratio, respectively), which could be separated by silica gel column chromatography. We next attempted to phosphitylate and acetylate (*in situ*) the remaining OH positions as reported previously for arabinonucleosides (Scheme 5b).[17] However, attempts to mono phosphitylate these isomers resulted in very poor conversion (<2%; rt) or the formation of multiple inseparable products if microwave irradiation was used.

Oligonucleotide Synthesis and Characterization. DNA and RNA decanucleotides containing an OxT unit at a central position were assembled by solid-phase synthesis on a controlled-pore glass (CPG) solid support (Table 1). Coupling of the OxT amidites ($\mathbf{P_1}$−$\mathbf{P_3}$) required extended reaction times (ca. 2 h vs 10−15 min for DNA or RNA amidites) using 5-ethylthio-1*H*-tetrazole (ETT) as the activator. Under these

https://doi.org/10.1021/acs.joc.1c02254
J. Org. Chem. 2022, 87, 2367−2379

conditions, coupling efficiencies were >95%. After chain assembly, the solid supports were treated with ammonium hydroxide (rt, 48 h) followed with NEt_3/HF (rt, 48 h), purified by HPLC, and desalted by size exclusion chromatography. The formation of oligonucleotides was confirmed by ESI mass spectrometry (Supporting Information).

UV Thermal Melting and CD Experiments. The influence on the thermal stability of various duplexes containing the OxT monomers was first evaluated by UV-thermal duplex denaturing studies. These novel monomers were evaluated in an oligonucleotide sequence previously studied by our group and others to compare the hybridization properties with various modifications (Tables 1 and 2).[18,19] The modifications were placed at a central position where the impact on duplex stability would be the highest.

Incorporation of any of the three OxT monomers in the middle of the RNA strand resulted in a substantial decrease (ΔT_m ranged from −12 to −18 °C) in melting temperature with either an RNA or DNA complement (Table 1). To investigate this phenomenon further, we incorporated the OxT modifications in the DNA strand of dsDNA and DNA−RNA duplexes (Table 1). Again, a substantial decrease of thermal stability was found for a single insertion of OxT in the dsDNA duplex (ΔT_m ranged from −4 to −16 °C), with OxT_1 exerting the greatest destabilization. In sharp contrast, OxT_3 and OxT_2 monomers were tolerated when placed in the DNA strand of DNA−RNA hybrids, with no change or only minor destabilization (ΔT_m −1 °C) observed, respectively. T_m curves for the DNA−RNA hybrids are shown in Figure 1A. Thermodynamic parameters (Table 2) extracted from the melting profiles revealed significant enthalpic stabilization in D-OxT_2 ($\Delta\Delta H$ = −62.3 kJ/mol) and D-OxT_3 ($\Delta\Delta H$ = −112.2 kJ/mol) modified duplexes, as compared to the unmodified counterpart. However, this stabilization is offset by reduced entropic contributions in the oxepane-modified duplexes ($\Delta\Delta S$ = −208.4 and −369.4 J/K/mol, respectively).

Circular dichroism spectroscopy was conducted on modified and unmodified DNA−RNA duplexes at 5 °C to analyze differences in helicity. In general, all oligonucleotides duplexed to RNA exhibited similar CD profiles giving evidence of A-type helices (Figure 1B, Figure S3). Interestingly, DNA−RNA duplexes containing OxT_2 and OxT_3 exhibited very similar spectra that are plausibly more A-form than the unmodified duplex, with more intense minima at 210 nm and less intense minima at 245 nm. On the other hand, the DNA−RNA duplex containing OxT_1 was most similar to the unmodified duplex, but the lower amplitude of the maximum peak at 265 nm is indicative of destabilization, thereby explaining the lower T_m value.

Structural Insights from Molecular Modeling and Dynamics Studies. From the melting studies, it is clear that duplex stability is retained only when the modification (OxT_2 and OxT_3) is incorporated into the DNA strand of a DNA−RNA hybrid duplex. By contrast, the OxT_1 modification is not tolerated in either DNA−RNA hybrid or DNA−DNA duplexes. To understand the atypical preference by the oxepane modification, MD simulations were carried out on 7 modified duplexes and 3 unmodified duplexes (DNA−DNA duplex (DD); DNA−RNA (DR, modification in DNA) duplex; RNA−DNA duplex (RD, modification in RNA) (Table 3). Briefly, the force field was developed for OxT modification (Figure S53, Supporting Information) using Gaussian16 and RED Tool III utilizing previously developed protocols[20,21] and was incorporated into duplexes using XLeap in AMBER 18.[22] After 500 ps of equilibration, the system was then subjected to 500 ns of production MD simulations using GPU accelerated version of AMBER 18.[23−25] Various structural and energetic parameters were calculated from the MD trajectories to rationalize the experimental observations.

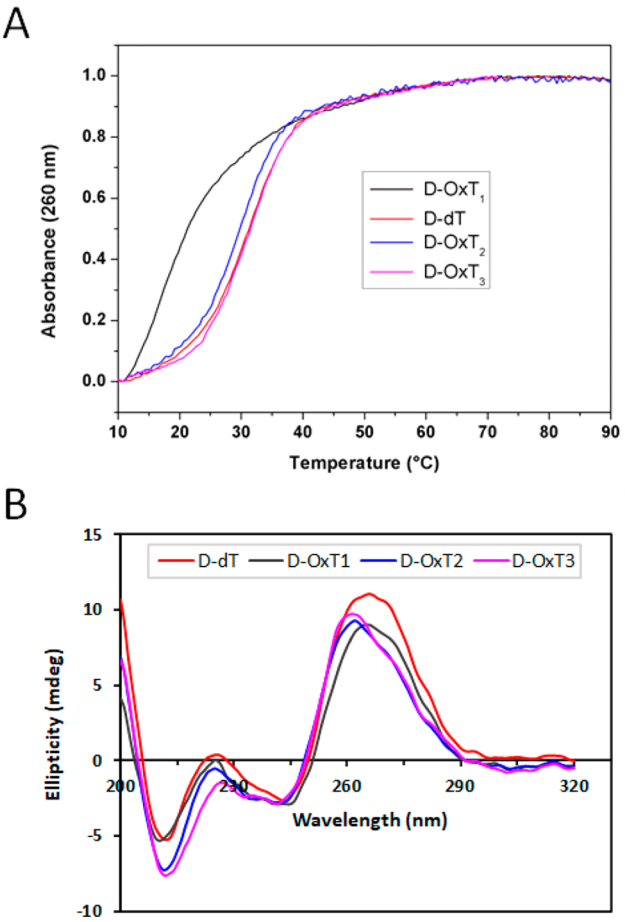

Figure 1. (A) Melting and (B) CD curves of modified DNA−RNA hybrids containing the OxT modifications in the DNA strand. UV samples were prepared in 10 mM sodium phosphate buffer (pH 7.3) containing 140 mM KCl and 1 mM $MgCl_2$ for a final concentration of 1.5 μM for each strand. CD samples were prepared at 25 μM, 5 mM sodium phosphate, 140 mM potassium chloride, and 1 mM magnesium chloride buffer, pH 7.3. Sequences of strands and their T_m values are provided in Table 1.

The root mean square deviation (RMSD) of backbone, bases, and the complete duplex for each system was calculated from the 500 ns trajectories. The overall RMSD and backbone of OxT_2 and OxT_3 modification in DR is <3 Å (Table S2, Supporting Information), indicating the helical geometry of the duplex is not deviated from both the initial structure and the unmodified duplex. However, the OxT_1 modification in DR was found to be highly flexible and seems to be largely distorted from the initial structure as indicated by higher deviations in the RMSD values. On the other hand, modifications in the RNA strand of RD duplex showed a higher RMS deviation of >5 Å (Table S2, Supporting Information). This indicates that there is significant distortion in the helical geometry of the duplex. RMSD of the position of modification and their adjacent nucleotides were calculated to find the relative stability of the modified position (Table S2, Supporting Information). The OxT_1 modification

https://doi.org/10.1021/acs.joc.1c02254
J. Org. Chem. 2022, 87, 2367−2379

Table 3. Nucleic Duplexes Used in MD Studies[a]

no.	sequence	modification	code
1	5′-d(CCATTATAGC)-3′ 3′-r(GGTAATATCG)-5′	unmodified	DR
2	5′-d(CCATXATAGC)-3′ 3′-r(GGTAATATCG)-5′	OxT-1	DR
3	5′-d(CCATXATAGC)-3′ 3′-r(GGTAATATCG)-5′	OxT-2	DR
4	5′-d(CCATXATAGC)-3′ 3′-r(GGTAATATCG)-5′	OxT-3	DR
5	5′-r(CCAUUAUAGC)-3′ 3′-d(GGTAATATCG)-5′	unmodified	RD
6	5′-r(CCAUXAUAGC)-3′ 3′-d(GGTAATATCG)-5′	OxT-1	RD
7	5′-r(CCAUXAUAGC)-3′ 3′-d(GGTAATATCG)-5′	OxT-2	RD
8	5′-r(CCAUXAUAGC)-3′ 3′-d(GGTAATATCG)-5′	OxT-3	RD
9	5′-d(CCATTATAGC)-3′ 3′-d(GGTAATATCG)-5′	unmodified	DD
10	5′-d(CCATXATAGC)-3′ 3′-d(GGTAATATCG)-5′	OxT-1	DD

[a]Nucleic acid sequences and position of the modifications used in the MD simulations studies. The positions of modification are underlined.

disrupts the adjacent nucleotides (>4 Å) in both DR (Figure 2B) and RD duplexes (Figure 3B).

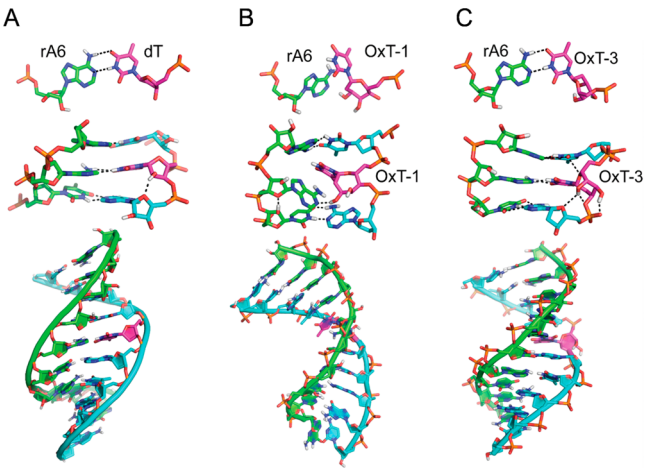

Figure 2. Representative structures of the major clusters of the (A) unmodified, (B) OxT_1-modified, and (C) OxT_3-modified DR systems from the 500 ns simulation trajectory. The position of modification is represented in magenta. The complementary nucleotide of the position of modification is represented as rA6. The images represent the modified position with the complementary base, adjacent bases, and the hybrid.

This can be attributed to the presence of the seven-membered ring, which tries to avoid a steric clash with nearby nucleotides. Due to the 4′-7′ and 3′-7′ linkage in the OxT_2 and OxT_3, respectively, they are suitably accommodated in the DNA strand without much fluctuation of the adjacent nucleotides (Figure 2 and Figure 4). Contrastingly, the modification of OxT_2 and OxT_3 along with their adjacent nucleotides are highly fluctuated (>4 Å) in the case of RD duplex (Table S2, Supporting Information). Notably, the observed structural fluctuations of the nucleotides are in line with the thermal stability of the

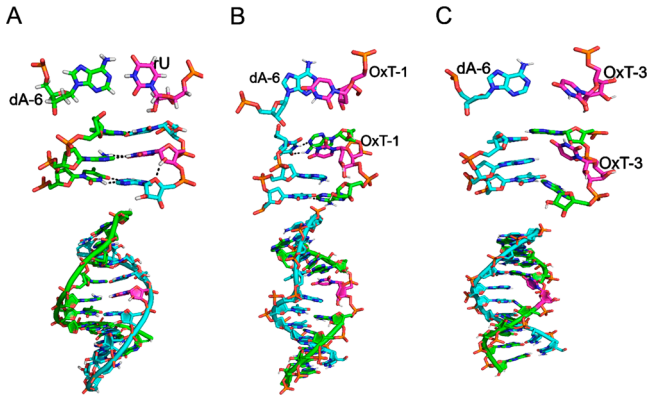

Figure 3. Representative structures of the major clusters of (A) unmodified, (B) OxT_1-modified, and (C) OxT_3-modified RD systems from the 500 ns simulation trajectory. The position of modification is represented in magenta. The complementary nucleotide of the position of modification is represented as dA6. The images represent the modified position with the complementary base, adjacent bases, and the hybrid.

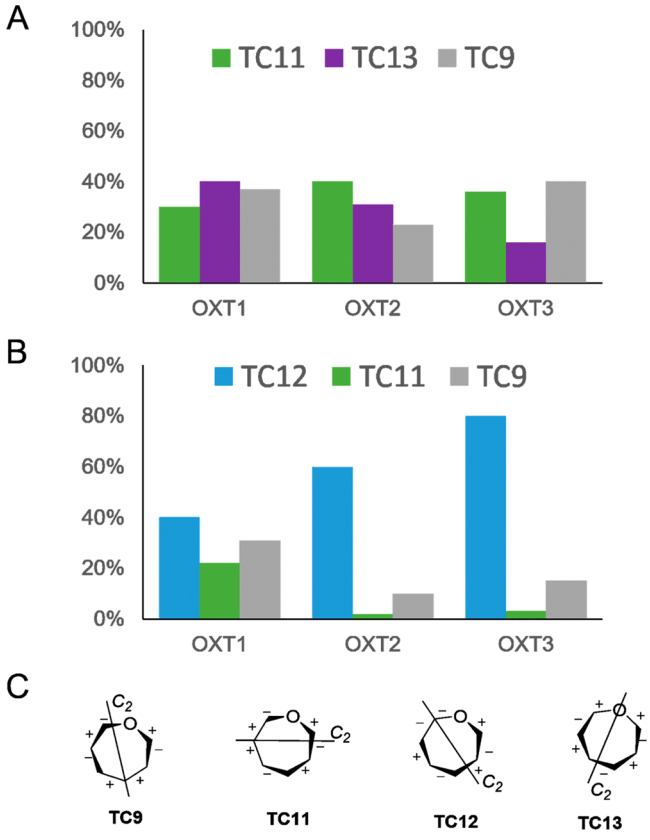

Figure 4. Conformational preferences of the oxepane nucleosides in (A) DR and (B) RD systems. The percentage occurrence of the conformers in OxT_1, OxT_2 and OxT_3 modifications is shown. TC9 is represented in gray. TC11 is represented in green. TC12 is represented in cyan. TC13 is represented in purple. (C) Structural representation of the major conformations observed during the MD simulations. C_2 denotes the pseudoaxis for each of the conformations, according to Entrena et al.[27]

modified DR and RD duplexes. To understand this further, we calculated W−C H-bond occupancy and C1′−C1′ distances for all the systems.

https://doi.org/10.1021/acs.joc.1c02254
J. Org. Chem. 2022, 87, 2367−2379

There is the presence of strong H-bond interaction between the modified nucleotide and the pairing rA base for OxT_2- and OxT_3-modified DR systems. The C1′−C1′ distance of OxT_2 and OxT_3 (<11 Å) (Table S4, Supporting Information) with their corresponding base-pairing atoms in DR duplexes reflect the same. The C1′−C1′ distance between the OxT_1 and rA nucleotides in the DR duplex and all of the OxT modifications in the RD duplex are found to be >14 Å, which does not favor the formation of W−C H-bonds (Table S4, Supporting Information). All the modifications in RD duplexes exhibited a low (<30%) W−C H-bond occupancy (Table S3, Supporting Information). The large C1′−C1′ distances and the low W−C H-bond percentage occupancies indicate a local base pair opening for the OxT_1 modification in both DR and RD duplexes (Figure 2 and Figure 3). Though this observation is consistent with the results from thermal melting studies, the local base pair opening events may be overestimated by AMBER force field parameters.[26]

Stacking interaction plays a significant role in the formation of the helical geometry and stability of the nucleic acid duplexes. To compare the relative stability of the stacking interactions, the stacking energy of the duplex was estimated using the MINT software package. Stacking energy for each duplex is shown in Table 4. Incorporation of a single OxT modification in RD duplex predominantly affects the stacking energy, which is found to be <15 kcal/mol. This value represents that the alignment of nucleobases in the RD duplex is affected due to the presence of modification. The stacking energy values of OxT_2 and OxT_3 modified DR duplexes are comparable to the unmodified DR duplex system with slight deviations, while the stacking energy of OxT_1 is −12.5 ± 4.7 (Table 4).

Table 4. Stacking Energies of Unmodified and Modified Duplexes[a]

modification	modified RNA/DNA	modified DNA/RNA
	5′-r(CCAUXAUAGC)-3′	5′-d(CCAUXAUAGC)-3′
	3′-d(GCTATAATGG)-5′	3′-r(GGTAATATCG)-5′
unmodified	−45.7 ± 8.9	−34.2 ± 6.7
OxT_1	−13.6 ± 8.8	−12.5 ± 4.7
OxT_2	−11.3 ± 7.4	−29.2 ± 2.9
OxT_3	−11.2 ± 5.2	−29.6 ± 3.7

[a]Stacking energies of unmodified and modified duplexes were calculated in kcal/mol using MINT software. Ten snapshots were obtained from every 50 ns interval from the MD trajectory. The stacking energy was calculated for each base pair, and then the final sum value for each snapshot was estimated.

To probe the possibility of H-bond between the additional hydroxyl group in oxepane (5′-OH and 7′-OH) and adjacent atoms (≤4 Å), the H-bond occupancies were calculated from the MD trajectories (Figure S61, Supporting Information). Interestingly, two H-bonds were observed between hydroxyl groups in OxT_3 and phosphate backbone toward the 5′-end of the modification as shown in Figure 2C. This H-bond was formed after 50 ns, and it was stable throughout MD simulations. To confirm this observation, two different MD simulations runs were performed. In both the runs, we observed this H-bond after 50−60 ns, which confirms its existence in DR duplexes. The H-bond distance between hydroxyl atoms (5′-OH and 7′-OH) and the oxygen atoms (OP1 and OP2) (Figure S61, Supporting Information) in the phosphate backbone of the DR system is found to be <3.1 Å (Figure S61, Supporting Information). The percentage occupancies of these H-bonds are >75%, and this reduces the flexibility of the atoms in the oxepane ring. Since in the OxT_1 modification, the hydroxyl groups are not close to the phosphate backbone (Figure S54, Supporting Information), such H-bonds were not observed in the DR duplexes. In the case of RD duplexes, the 5′-OH and 7′-OH groups of the OxT_2 and OxT_3 modification in RNA strand also make H-bond interaction with the backbone of the RNA, but the H-bond occupancies are found to be <12% of simulation time. It is interesting to note that the H-bond between oxepane ring and phosphate backbone is observed only when the modification is present in the DNA strand. This can be attributed to (i) differences between the phosphodiester backbone angle of DNA and RNA strands, arising from different conformational preferences of corresponding sugars (C2′-*endo* in DNA and C3′-*endo* in RNA) and (ii) motion of the backbone dihedral angles in the 5′-end adjacent nucleotides, which also influences the flexibility of the oxepane ring atoms in OxT_2 and OxT_3 modifications.

The sugar conformational space of the oxepane ring is represented by a twisted-chair conformation as reported previously.[27] The QM energy optimization (B3LYP-D3 in Gaussian16) of the oxepane nucleoside resulted in TC9, TC10, TC12, and TC14 as their low energy conformers.[28] The oxepane modifications adopt the TC9, TC11, and TC13 conformations in the RNA strand of RD duplex (Figure 4). This indicates that the modification is flexible in the RD duplex. The sugar conformation of adjacent RNA ribonucleotides is found to be in North C3′-*endo* puckering, as expected. In the case of OxT_2 and OxT_3 modifications in the DR system, the primary conformation of the oxepane ring is TC12 along with minor sampling at TC11 and TC9 conformers (Figure 4). Additionally, the TC12 conformer is optimal for the oxepane hydroxyl atom to make H-bond interaction with the adjacent phosphate backbone toward the 5′-end direction. Such TC12 conformation is not seen while the OxT modification is present in the RNA strand of the RD duplex; instead, TC9 and TC11 were observed. These observations clearly show that the backbone dihedral angle preference of the RNA strand influences the conformational preference of the OxT modifications. The dihedral angle preference of the DNA strand allows the accommodation of the oxepane modification into the system and enables the backbone H-bond interaction. This is reflected in the favorable enthalpy contributions revealed from the UV melting studies.

The probability distribution for α, β, γ, δ, ε, ζ, and χ dihedral angles were compared with the unmodified systems (Figures S54−S56, Supporting Information). The backbone dihedral features of the unmodified DNA strand of the DR duplex indicates the DNA strand exists in the B_I and B_{II}[29] type conformation in a DR duplex, and the typical B-type backbone dihedral values are not seen. OxT_3 modification in the DR duplex has different backbone dihedral preferences compared to the unmodified duplex. The γ, δ, ζ, ε, κ, and λ glycosidic dihedral angle preferences in the DNA strand of DR duplex helps to tolerate the modification, while these angle preferences in the RNA strand of RD prevents the tolerance of the oxepane modifications.. The six local base parameters and the six local base pair step parameters were computed to see the behavior of the modification within the duplex strands (Figure S57 and Figure S58, Supporting Information). These parameters in the DR and RD duplex are different, which implies that both helical bending as well as base orientation changes occur upon introducing these modifications in the RNA strands.

https://doi.org/10.1021/acs.joc.1c02254
J. Org. Chem. 2022, 87, 2367−2379

An OxT_1 modified DD system was studied to probe the tolerance of oxepane modifications in the DNA strand of the DNA−DNA duplexes. The O4−N6 and the N3−N1 H-bond occupancies in the modified DD duplex were 2% and 4%, respectively, while the same for the unmodified DD duplex were 96% and 99%, respectively. The C1′−C1′ distance was 16.3 ± 2.1 Å, which does not favor the formation of a stable W−C H-bond. Finally, the stacking energy of the OxT_1 modified DD system was found to be 12 ± 7.4 kcal/mol, which is a low value indicating the absence of a strong stacking interaction to maintain the helical geometry and stability of the duplex. These factors evidently suggest that the oxepane modification inclusion in the DNA−DNA duplex affects the stability of the system, in line with the results obtained from the melting studies.

In conclusion, our work provides methods and conditions for the functionalization of oxepane nucleosides with control of chemo-, regio-, and stereoselectivity. Furthermore, our MD studies delineate the atomistic details and rationale on the effect of OxT modifications in the structural stability of duplexes. In conjunction with UV denaturation studies, they revealed that OxT_2 and OxT_3 are suitable to be incorporated in the DNA strand of hybrid duplexes due to their favorable structural and functional features, such as dihedral angle preferences and H-bond interactions. Together, they account for a rare type of "DNA-like" modification that, on the one hand, is well accommodated inside DNA−RNA hybrids, thereby with potential applications in xenobiology,[1] and antisense[30] and CRISPR technologies,[31] and, on the other hand, expands the "toolbox" of modifications that nucleic acid chemists and biologists can experiment with.

EXPERIMENTAL SECTION

All laboratory-grade chemicals and solvents were obtained from commercial suppliers and were used without further purification. Thin-layer chromatography (TLC) was performed on TLC aluminum sheets covered with silica gel 60 F_{254} (0.2 mm). Silica gel 60 (40−60 μM) was used for flash column chromatography (FC). Microwave-assisted reactions were conducted in a Biotage Initiator instrument, in sealed 1 mL microwave reaction vials at 90 °C for 1 h. HRMS data were obtained by ESI-MS using a Thermo Scientific Exactive Plus Orbitrap mass spectrometer or a Bruker Daltonics Maxis Impact quadrupole time-of-flight (QTOF) mass spectrometer. A suitable crystal was selected and measured on a Bruker Venture Metaljet diffractometer. The crystal was kept at 150 K during data collection. The structure was solved with the ShelXT structure solution program using intrinsic phasing and refined with the XL refinement package using least squares minimization.[13] Structural assignments of nucleosides were obtained from gCOSY, gHSQC, and gHMBC NMR experiments.

(1*R*)-1-[(3*S*,4*S*,5*S*,6*R*)-2-Deoxy-3,4-dihydroxy-5,7-di-*tert*-butylsilanediyl)-β-oxepinyl]thymine (5). To a solution of 4[7] (204 mg, 0.5 mmol) in *tert*-butyl alcohol (2.5 mL) and water (2.5 mL) at 0 °C was added AD-mix-α (700 mg) at 0 °C. The reaction mixture was stirred at the same temperature for 16 h, after which Na_2SO_3 (750 mg) and then water (10 mL) were added at room temperature. This was followed by extraction with ethyl acetate. The combined organic layers were dried over anhydrous Na_2SO_4 and rotoevaporated under reduced pressure. The material left was purified by flash column chromatography on silica gel using a solution of CH_2Cl_2/MeOH (96:4, v/v) as the eluent. Nucleoside **5** (186 mg, 0.42 mmol, 84%) was isolated as a white solid. R_f = 0.49, CH_2Cl_2/MeOH (9:1, v/v). Crystals of this nucleoside suitable for X-ray diffraction were obtained by dissolving **5** in 0.5 mL of MeOH and then making up different solutions of **5 in** MeOH:CH_2Cl_2 (10:1 to 1:1 range, v/v). Nucleoside **5** crystallized upon standing in one of these solutions (CCDC no. 2108264). ^{1}H NMR ($CDCl_3$, 500 MHz): δ 9.03 (1H, s, NH), 7.16 (1H, s, H-6), 6.08 (1H, t, *J* = = 6.7 Hz, 1′-H), 4.26 (1H, s, 4′-H), 4.20−4.15 (1H, m, 3′-H), 4.11 (1H, dd, *J* = = 10.5/4.9 Hz, 7′-H), 4.01−3.92 (2H, m, 5′-H and 6′-H), 3.76 (1H, t, *J* = = 9.9 Hz, 7′- H), 3.00 (1H, d, *J* = = 1.6 Hz, 3′-OH), 2.91 (1H, d, *J* = = 8.3 Hz, 4′-OH), 2.56 (1H, ddd, *J* = = 15.2/9.3/6.2 Hz, 2′-$H_α$), 2.16−2.11 (1H, m, 2′-$H_β$), 1.92 (3H, s, CH_3), 1.04 (9H, s, Si(CH_3)$_3$), 1.01 (9H, s, Si(CH_3)$_3$). ^{13}C{^{1}H} NMR ($CDCl_3$, 125 MHz): δ 163.8 (1C, C-4), 150.0 (1C, C-2), 135.4 (1C, C-6), 111.5 (1C, C-5), 82.3 (1C, C-1′), 77.5 (1C, C-4′), 76.8 (1C, C-5′), 73.8 (1C, C-6′), 68.0 (1C, C-3′), 66.8 (1C, C-7′), 37.3 (1C, C-2′), 27.6 (3C, Si(CH_3)$_3$), 27.3 (3C, Si(CH_3)$_3$), 22.8 (1C, C(CH_3)$_3$), 20.3 (1C, C(CH_3)$_3$), 12.8 (1C, CH_3). HRMS (*m*/*z*): [M − H]$^-$ calcd for $C_{20}H_{33}O_7N_2Si$, 441.2062; found, 441.2064.

(1*R*)-1-[(3*S*,4*S*,5*S*,6*R*)-2-Deoxy-3-acetyl-4-hydroxy-5,7-di-*tert*-butylsilanediyl)-β-oxepinyl]thymine (6). To a solution of **5** (200 mg, 0.45 mmol) in dry pyridine (5 mL) were added acetic anhydride (43 μL, 0.45 mmol) and 4-dimethylaminopyridine (3 mg, 0.24 mmol). The reaction was stirred at room temperature for 1 h, after which water (20 mL) and saturated aqueous $NaHCO_3$ (5 mL) were added. This was followed by extraction with ethyl acetate (3 × 100 mL). The combined organic layers were dried over anhydrous Na_2SO_4 and rotoevaporated under reduced pressure. The material left was purified by flash column chromatography on silica gel using a solution of hexane/EtOAc (1:4, v/v) as the eluent. Compound **6** (175 mg, 0.36 mmol, 80%) was isolated as a white solid. R_f = 0.47, hexane/EtOAc (4:6, v/v). ^{1}H NMR ($CDCl_3$, 500 MHz): δ 8.71 (1H, s, NH), 7.38 (1H, d, *J* = = 1.2 Hz, H-6), 6.13 (1H, t, *J* = = 6.8 Hz, 1′-H), 5.25 (1H, dd, *J* = = 10.3/5.3 Hz, 3′-H), 4.23 (1H, s, 4′-H), 4.15−4.09 (1H, m, 7′-H), 3.95 (1H, dd, *J* = = 9.6/2.6 Hz, 5′-H), 3.90 (1H, td, *J* = = 9.8/5.0 Hz, 6′-H), 3.76 (1H, t, *J* = = 10.1 Hz, 7′-H), 2.74 (1H, ddd, *J* = = 14.7/10.3/7.4 Hz, 2′-Hα), 2.65 (1H, brs, 4′-OH), 2.11 (3H, s, COCH_3), 2.10−2.05 (1H, m, 2′-$H_β$), 1.95 (3H, d, *J* = = 1.1 Hz, CH_3), 1.04 (9H, s, Si(CH_3)$_3$), 1.01 (9H, s, Si(CH_3)$_3$). ^{13}C{^{1}H} NMR ($CDCl_3$, 125 MHz): δ 170.7 (1C, $COCH_3$), 163.5 (1C, C-4), 150.0 (1C, C-2), 135.6 (1C, C-6), 111.9 (1C, C-5), 81.6 (1C, C-1′), 76.8 (1C, C-5′), 75.0 (1C, C-4′), 73.6 (1C, C-6′), 69.8 (1C, C-3′), 66.6 (1C, C-7′), 32.6 (1C, C-2′), 27.5 (3C, Si(CH_3)$_3$), 27.3 (3C, Si(CH_3)$_3$), 22.8 (1C, C(CH_3)$_3$), 21.3 (1C, $COCH_3$), 20.3 (1C, C(CH_3)$_3$), 12.7 (1C, CH_3). HRMS (*m*/*z*): [M − H]$^-$ calcd for $C_{22}H_{35}O_8N_2Si$, 483.2168; found, 483.2167.

(1*R*)-1-[(3*S*,4*S*,5*R*,6*R*)-2-Deoxy-3-*O*-dimethyltertbutylsilyl-4-acetyl-5,7-di-*tert*-butylsilanediyl)-β-oxepinyl]thymine (7). To a solution of **6** (80 mg, 0.165 mmol) in dry pyridine (3 mL) and DMF (3 mL) was added *t*-butyldimethylsilyl chloride (124 mg, 0.82 mmol) and imidazole (56 mg, 0.82 mmol). The reaction mixture was stirred at room temperature at 120 °C for 16 h. Water (100 mL) was added, and the resulting mixture extracted with ethyl acetate. The combined organic layers were dried over (Na_2SO_4) and filtered, and the solvent was removed *in vacuo*. The residue was purified by flash column chromatography on silica gel using a solution of hexane/EtOAc (2.5:1, v/v) to give **7** as a white solid (71 mg, 0.118 mmol, 72%). R_f = 0.42, hexane/EtOAc (9:1, v/v). ^{1}H NMR ($CDCl_3$, 500 MHz): 8.47 (1H, s, NH), 7.12 (1H, d, *J* = = 1.2 Hz, H-6), 6.15 (1H, dd, *J* = = 8.1/6.1 Hz, 1′-H), 5.53 (1H, d, *J* = = 1.9 Hz, 4′-H), 4.21 (1H, ddd, *J* = = 7.4/6.2/1.0 Hz, 3′-H), 4.14−4.08 (1H, m, 7′-H), 4.01 (1H, dd, *J* = = 9.7/2.9 Hz, 5′-H), 3.90 (1H, td, *J* = = 10.0/5.1 Hz, 6′-H), 3.76 (1H, t, *J* = = 10.3 Hz, 7′-H), 2.38 (1H, ddd, *J* = = 14.7/8.7/6.1 Hz, 2′-H), 2.17 (3H, s, COCH_3), 2.03−1.98 (1H, m, 2′- $H_β$), 1.95 (3H, d, *J* = = 1.1 Hz, CH_3), 1.03 (9H, s, Si(CH_3)$_3$), 0.95 (9H, s, Si(CH_3)$_3$), 0.87 (9H, s, TBDMS), 0.12 (3H, s, TBDMS), δ 0.07 (3H, s, TBDMS). ^{13}C{1H} NMR ($CDCl_3$, 125 MHz): δ 169.5 (1C, $COCH_3$), 163.4 (1C, C-4), 149.7 (1C, C-2), 135.0 (1C, C-6), 111.8 (1C, C-5), 82.5 (1C, C-1′), 78.5 (1C, C-4′), 75.9 (1C, C-5′), 75.5 (1C, C-6′), 67.9 (1C, C-3′), 66.8 (1C, C-7′), 39.3 (1C, C-2′), 27.5 (3C, Si(CH_3)$_3$), 27.0 (3C, Si(CH_3)$_3$), 25.8 (3C, TBDMS), 22.8 (1C, C(CH_3)$_3$), 21.2 (1C, $COCH_3$), 20.1 (1C, C(CH_3)$_3$), 14.3 (1C, TBDMS), 12.7 (1C, CH_3), −4.7 (2C, TBDMS). HRMS (*m*/*z*): [M + Na]$^+$ calcd for $C_{28}H_{50}O_8N_2Si_2Na$, 621.2998; found, 621.3007.

1-[(3*R*,4*S*,5*R*,6*R*)-2-Deoxy-3,5-dihydroxy-3-*O*-*tert*-butyldimethylsilyl-4-acetyl-7-*O*-(4,4′-dimethoxytrityl)-β-oxepanyl]-thymine (8). To a solution of **7** (718 mg, 1.20 mmol) in dry pyridine (3 mL) and THF (3 mL) was added pyridine-HF (500 μL). The reaction mixture was stirred for 15 min at 0 °C. After completion of the reaction (checked by TLC), the solvent was removed *in vacuo* to form diol (confirmed with mass spectrometry) (note that either heating or

https://doi.org/10.1021/acs.joc.1c02254
J. Org. Chem. 2022, 87, 2367−2379

prolonged fluoride treatment should be avoided as it leads to significant cleavage of the 3′-TBDMS group). Then the diol (500 mg, 1.09 mmol) is coevaporated with dry pyridine (5 mL) three times, and then pyridine (5 mL) was added to it. DMTr-Cl (425 mg, 1.24 mmol) was added in three portions to the reaction mixture and was stirred at an ambient temperature for 3 h. Dichloromethane (10 mL) and $NaHCO_3$ (20 mL) were added, and the resulting mixture was extracted with dichloromethane. The combined organic layers were dried over anhydrous Na_2SO_4 and filtered, and the solvent was removed *in vacuo*. The material left was purified by flash column chromatography on silica gel using a solution of hexane/EtOAc (5:3, v/v) as the eluent. Nucleoside **8** (493 mg, 0.64 mmol, 54% yield over two steps) was isolated as white solid foam. R_f = 0.40, hexane/EtOAc (5:4, v/v). ^{1}H NMR (DMSO-d_6, 500 MHz): δ 11.44 (1H, s, NH), 7.89 (1H, d, J = 1.04 Hz, H-6), 7.35−7.33 (2H, m, DMTr), 7.25−7.17 (7H, m, DMTr), 6.83−6.79 (4H, m, DMTr), 6.22 (1H, dd, J = 10.2/5.0 Hz, 1′-H), 5.19 (1H, d, J = 3.6 Hz, 4′-H), 4.86 (1H, d, J = 6.9 Hz, 5′-OH), 4.27 (1H, t, J = 6.5 Hz, 3′-H), 3.87−3.82 (1H, m, 6′-H), 3.72 (6H, DMTr), 3.60 (1H, ddd, J = 10.0/7.0/3.6 Hz, 5′-H), 3.40−3.38 (1H, m, 7′-H), 3.00−2.98 (1H, m, 7′-H), 2.45 (1H, ddd, J = 13.9/10.3/5.3 Hz, 2′-H$_\beta$), 2.08 (3H, s, $COCH_3$), 1.94 (1H, ddd, J = 12.7/7.3/5.0 Hz, 2′-H$_\alpha$), 1.87 (3H, s, CH_3), 0.86 (9H, s, TBDMS), 0.10 (3H, s, TBDMS), 0.08 (3H, s, TBDMS). ^{13}C{^{1}H} NMR (DMSO-d_6, 125 MHz): δ 169.4 (1C, $COCH_3$), 163.8 (1C, C-4), 157.9 (2C, DMTr), 150.3 (1C, C-2), 145.1 (1C, DMTr), 136.9 (1C, C-6), 135.9 (2C, DMT), 129.6 (2C, DMTr), 129.5 (2C, DMT), 127.7 (4C, DMTr), 126.5 (1C, DMTr), 113.0 (4C, 1C C-5 and 3C DMTr), 109.5 (1C, DMTr), 84.8 (1C, DMTr), 82.8 (1C, 6′-C), 82.5 (1C, 1′-C), 78.7 (1C, 4′-C), 69.3 (1C, 3′-C), 68.9 (1C, 5′-C), 55.0 (2C, 2 × OCH_3), 64.5 (1C, 7′-C), 38.2 (1C, 2′-C), 25.6 (3C, TBDMS), 20.9 (1C, $COCH_3$), 17.6 (1C, TBDMS), 12.1 (1C, CH_3), −4.9 (1C, TBDMS), −5.0 (1C, TBDMS). HRMS (m/z): [M + Na]$^+$ calcd for $C_{41}H_{52}O_{10}N_2SiNa$, 783.3283; found, 783.3273.

1-[(5*S*,6*R*)-2-Deoxy-5-hydroxy-3,4-ene-7-*O*-(4,4′-dimethoxytrityl)-*β*-oxepenyl]thymine (10). Compound **9**[7] (152 mg, 0.57 mmol) was dried by coevaporation with dry pyridine (3 × 5 mL). Pyridine (4 mL) was added, followed by three portions of DMTrCl (231 mg, 0.68 mmol total), and the resulting reaction mixture was stirred at an ambient temperature for 3 h. Dichloromethane (10 mL) was added, followed by saturated aq $NaHCO_3$ (20 mL), and the product extracted with dichloromethane (3 × 20 mL). The combined organic layers were dried over (Na_2SO_4) and filtered, and the solvent was removed under reduced pressure. The material left was purified by flash column chromatography on silica gel using solution of hexane/EtOAc (5:3, v/v) as the eluent. Nucleoside **10** (195 mg, 0.34 mmol, 60%) was isolated as a white solid foam. R_f = 0.40, hexane/EtOAc (5:4, v/v). ^{1}H NMR (DMSO-d_6, 500 MHz): δ 11.45 (s, NH), 7.84 (1H, d, J = 1.12 Hz, H-6), 7.37−7.36 (2H, m, DMTr), 7.25−7.17 (7H, m, DMTr), 6.82−6.80 (4H, m, DMTr), 5.83 (1H, dd, J = 10.7/2.1 Hz, 1′-H), 5.68 (1H, dt, J = 12.7/2.3 Hz, 4′-H), 5.64−5.59 (1H, m, 3′-H), 5.12 (1H, d, J = 7.51 Hz, 5′-OH), 3.94−3.91 (1H, m, 5′-H), 3.72 (6H, s, DMTr), 3.64−3.61 (1H, m, 6′-H), 3.13 (1H, dd, J = 9.7/1.9 Hz,7′-H), 3.04 (1H, dd, J = 9.7/7.8 Hz,7′-H), 2.96−2.90 (1H, m, 2′-H$_\beta$), 2.39 (1H, ddd, J = 9.3/7.4/1.9 Hz, 2′-H$_\alpha$), 1.85 (3H, s, CH_3). ^{13}C{^{1}H} NMR (DMSO-d_6, 125 MHz): δ 163.8 (1C, C-4), 157.9 (1C, DMTr), 150.3 (1C, C-2), 145.1 (1C, DMTr), 137.5 (4′-C), 136.6 (C-6), 136.0 (1C, DMTr), 135.8 (1C, DMTr), 129.7 (2C, DMT), 129.6 (2C, DMTr), 127.7 (2C, DMTr), 127.6 (2C, DMTr), 126.5 (1C, DMTr), 122.6 (3′-C), 113.0 (4C, DMTr), 109.2 (1C, C-5), 84.8 (1C, DMTr), 84.0 (1C, 6′-C), 83.9 (1C, 1′-C), 69.5 (1C, 5′-C), 64.3 (1C, 7′-C), 55.0 (2C, 2 ×OCH_3), 34.5 (1C, 2′-C), 12.1 (1C, CH_3). HRMS (m/z): [M + Na]$^+$ calcd for $C_{33}H_{34}N_2O_7Na$, 593.2298; found, 593.2244.

1-[(5*S*,6*R*)-2-Deoxy-5-*O*-*tert*-butylsilyl-3,4-ene-7-*O*-(4,4′-dimethoxytrityl)-*β*-oxepenyl]thymine (11). To a solution of **10** (100 mg, 0.17 mmol) in dry DMF (2 mL) were added TBDMSCl (77 mg, 0.51 mmol) and imidazole (75 mg, 0.51 mmol). The reaction mixture was stirred at an ambient temperature for 16 h, after which water (10 mL) and saturated aq $NaHCO_3$ (20 mL) were added. This was followed by extraction with ethyl acetate (3 × 20 mL). The combined organic layers were dried over anhydrous Na_2SO_4 and rotoevaporated under reduced pressure. The material left was purified by flash column chromatography on silica gel using a solution of hexane/EtOAc (5:4, v/v) as the eluent. Compound **11** (110 mg, 0.16 mmol, 94%) was isolated as a white solid. R_f = 0.32, hexane/EtOAc (5:4, v/v). ^{1}H NMR (DMSO-d_6, 500 MHz): δ 11.46 (s, NH), 7.84 (1H, d, J = 1.10 Hz, H-6), 7.38−7.36 (2H, m, DMTr), 7.26−7.16 (7H, m, DMTr), 6.81−6.78 (4H, m, DMTr), 5.88 (1H, dd, J = 8.5/2.1 Hz, 1′-H), 5.72−5.67 (1H, m, 3′-H), 5.61 (1H, dt, J = 12.7/2.3 Hz, 4′-H), 4.12 (1H, dd, J = 9.2/2.0 Hz, 5′-H), 3.71 (6H, s, DMTr), 3.67 (1H, dd, J = 9.3/2.3 Hz, 6′-H), 3.04−2.95 (3H, m, 2′-H and 7′-H), 2.42 (1H, ddd, J = 9.6/7.5/1.9 Hz, 2′-H$_\alpha$), 1.87 (3H, s, CH_3), 0.64 (9H, s, TBDMS), −0.06 (3H, s, TBDMS), −0.28 (3H, s, TBDMS). ^{13}C{^{1}H} NMR (DMSO-d_6, 125 MHz): δ 163.8 (1C, C-4), 158.0 (3C, DMTr), 150.3 (1C, C-2), 145.0 (1C, DMTr), 136.6 (1C, 4′-C), 136.0 (1C, C-6), 135.5 (1C, DMTr), 129.6 (2C, DMTr), 127.6 (6C, DMTr), 126.5 (1C, DMTr), 123.7 (1C, 3′-C), 113.0 (4C, DMTr), 109.2 (1C, C-5), 84.8 (1C, DMTr), 84.7 (1C, 6′-C), 83.7 (1C, 1′-C), 70.9 (1C, 5′-C), 64.2 (1C, 7′-C), 55.0 (2C, 2 × OCH_3), 34.2 (1C, 2′-C), 25.4 (3C, TBDMS), 17.3 (1C, TBDMS), 12.1 (1C, CH_3), −4.5 (1C, TBDMS), −5.5 (1C, TBDMS). HRMS (m/z): [M + Na]$^+$ calcd for $C_{39}H_{48}N_2O_7SiNa$, 707.3123; found, 707.3132.

1-[(3*S*,4*S*,5*S*,6*R*)-2-Deoxy-3,4-dihydroxy-5-*O*-*tert*-butyldimethylsilyl-7-*O*-(4,4′-dimethoxytrityl)-*β*-oxepanyl]thymine (12). To a solution of **11** (103 mg, 0.15 mmol) in acetone (5 mL) and water (1 mL) were added osmium tetroxide (20 μL, 2.5% in ^{t}BuOH) and 4-methyl morpholin-4-oxide (NMO) (25 mg, 0.21 mmol) at 0 °C. The reaction mixture was stirred at the same temperature for 16 h, after which Na_2SO_3 (750 mg) followed by water (10 mL) was added at room temperature. This was followed by extraction with ethyl acetate. The combined organic layers were dried over anhydrous Na_2SO_4 and rotoevaporated under reduced pressure. The material left was purified by flash column chromatography on silica gel using a solution of CH_2Cl_2/MeOH (96:4, v/v) as the eluent. Nucleoside **12** (86 mg, 0.12 mmol, 80%) was isolated as a white solid. R_f = 0.44, CH_2Cl_2/MeOH (9:1, v/v). ^{1}H NMR (DMSO-d_6, 500 MHz): δ 11.41 (1H, s, NH), 7.85 (1H, d, J = 0.90 Hz, H-6), 7.33−7.31 (2H, m, DMTr), 7.23−7.15 (7H, m, DMTr), 6.81−6.78 (4H, m, DMTr), 6.13 (1H, dd, J = 10.0/6.3 Hz, 1′-H), 4.79 (1H, d, J = 4.30 Hz, 4′-OH), 4.78 (1H, d, J = 5.10 Hz, 3′-OH), 3.98−3.93 (1H, m, 3′-H), 3.91−3.88 (1H, m, 6′-H), 3.87−3.85 (1H, m, 4′-H), 3.71 (6H, s, DMTr), 3.40 (1H, dd, J = 9.8/1.9 Hz, 5′-H), 2.91−2.86 (2H, m, 7′-H), 2.42 (1H, ddd, J = 13.4/10.1/7.2 Hz, 2′-H$_\beta$), 1.95 (1H, ddd, J = 13.7/8.7/6.2 Hz, 2′-H$_\alpha$), 1.86 (3H, s, CH_3), 0.61 (9H, s, TBDMS), −0.05 (3H, s, TBDMS), −0.32 (3H, s, TBDMS). ^{13}C{^{1}H} NMR (DMSO-d_6, 125 MHz): δ 163.8 (1C, C-4), 157.9 (2C, DMTr), 150.6 (1C, C-2), 145.1 (1C, DMTr), 136.8 (1C, C-6), 136.1 (1C, DMTr), 135.6 (1C, DMTr), 129.5 (2C, DMTr), 129.4 (2C, DMTr), 127.7 (2C, DMTr), 127.6 (2C, DMTr), 126.4 (1C, DMTr), 113.0 (4C, 1C C-5 and 3C DMTr), 109.5 (1C, DMTr), 84.7 (1C, DMTr), 82.2 (1C, 1′-C), 81.7 (1C, 6′-C), 78.9 (1C, 4′-C), 72.6 (1C, 5′-C), 67.9 (1C, 3′-C), 64.3 (1C, 7′-C), 54.5 (2C, 2 ×OCH_3), 36.3 (1C, 2′-C), 25.6 (3C, TBDMS), 17.4 (1C, TBDMS), 12.1 (1C, CH_3), −4.2 (1C, TBDMS), −5.5 (1C, TBDMS). HRMS (m/z): [M + Na]$^+$ calcd for $C_{39}H_{50}N_2O_9SiNa$, 741.3177; found, 741.3169.

1-[(3*S*,4*S*,5*S*,6*R*)-2-Deoxy-3-acetyl-4-hydroxy-5-*O*-*tert*-butyldimethylsilyl-7-*O*-(4,4′-dimethoxytrityl)-*β*-oxepanyl]thymine (13) and 1-[(3*S*,4*S*,5*S*,6*R*)-2-Deoxy-3-hydroxy-4-acetyl-5-*O*-*tert*-butyldimethylsilyl-7-*O*-(4,4′-dimethoxytrityl)-*β*-oxepanyl]thymine (14). To a solution of **12** (90 mg, 0.125 mmol) in dry pyridine (1 mL) were added acetic anhydride (12 μL, 0.125 mmol) and 4-dimethylaminopyridine (3 mg, 0.24 mmol). The reaction mixture was stirred at room temperature for 2 h, after which water (10 mL) and saturated aq $NaHCO_3$ (5 mL) were added. This was followed by extraction with ethyl acetate (3 × 100 mL). The combined organic layers were dried over anhydrous Na_2SO_4 and rotoevaporated under reduced pressure. The material left was purified by flash column chromatography on silica gel using a solution of CH_2Cl_2/MeOH (98:2, v/v) as the eluent. Compound **13** (75 mg, 0.098 mmol, 78%) was isolated as a white solid, R_f = 0.48, CH_2Cl_2/MeOH (9:1, v/v), and separately along with compound **14** (8 mg, 0.01 mmol, 8%) as a white solid. R_f = 0.47, CH_2Cl_2/MeOH (9:1, v/v). Experimental data for **13**, ^{1}H NMR (DMSO-d_6, 500 MHz): δ 11.45 (1H, s, NH), 7.85 (1H, d, J = 0.92 Hz, H-6), 7.34−7.32 (2H, m, DMTr), 7.24−7.16 (7H, m, DMTr),

https://doi.org/10.1021/acs.joc.1c02254
J. Org. Chem. 2022, 87, 2367−2379

6.81−6.79 (4H, m, DMTr), 6.35 (1H, dd, J = 9.7/6.5 Hz, 1′-H), 5.55 (1H, d, J = 4.85 Hz, 4′-OH), 5.06 (1H, t, J = 8.1 Hz, 3′-H), 3.92−3.88 (1H, m, 6′-H), 3.71 (6H, s, DMTr), 3.47 (1H, dd, J = 9.8/1.9 Hz, 5′-H), 2.95−2.89 (2H, m, 7′-H), 2.55−2.52 (1H, m, 2′-H_β), 2.17−2.11 (1H, m, 2′-H_α), 2.04 (3H, s, $COCH_3$), 1.86 (3H, s, CH_3), 0.60 (9H, s, TBDMS), −0.08 (3H, s, TBDMS), −0.32 (3H, s, TBDMS). $^{13}C\{^1H\}$ NMR (DMSO-d_6, 125 MHz): δ 170.0 (1C, $COCH_3$), 163.8 (1C, C-4), 158.0 (2C, DMTr), 150.5 (1C, C-2), 145.0 (1C, DMTr), 136.8 (1C, C-6), 136.0 (1C, DMTr), 135.5 (1C, DMTr), 129.5 (2C, DMTr), 129.4 (2C, DMTr), 127.7 (2C, DMTr), 127.6 (2C, DMTr), 126.4 (1C, DMTr), 113.1 (4C, 1C C-5 and 3C DMTr), 109.7 (1C, DMTr), 84.8 (1C, DMTr), 81.8 (1C, 1′-C), 81.6 (1C, 6′-C), 75.3 (1C, 4′-C), 72.2 (1C, 5′-C), 71.7 (1C, 3′-C), 64.1 (1C, 7′-C), 54.5 (2C, 2 ×OCH_3), 32.8 (1C, 2′-C), 25.6 (3C, TBDMS), 21.7 (1C, $COCH_3$), 17.3 (1C, TBDMS), 12.1 (1C, CH_3), −4.4 (1C, TBDMS), −5.6 (1C, TBDMS). HRMS (m/z): $[M-H]^-$ calcd for $C_{41}H_{51}N_2O_{10}Si$, 759.33185; found, 759.3315. Experimental data for **14**, ^1H NMR (DMSO-d_6, 500 MHz): δ 11.47 (1H, s, NH), 7.90 (1H, d, J = 1.10 Hz, H-6), 7.34−7.32 (2H, m, DMTr), 7.23−7.15 (7H, m, DMTr), 6.81−6.78 (4H, m, DMTr), 6.23 (1H, dd, J = 9.2/6.8 Hz, 1′-H), 5.32 (1H, d, J = 2.59 Hz, 4′-H), 5.02 (1H, d, J = 5.8 Hz, 3′-OH), 4.19−4.14 (1H, m, 3′-H), 3.78−3.72 (1H, m, 6′-H), 3.71 (6H, s, DMTr), 3.63 (1H, dd, J = 9.7/2.6 Hz, 5′-H), 2.93−2.90 (1H, m, 7′-H), 2.82−2.80 (1H, m, 7′-H), 2.51−2.50 (1H, m, 2′-H_β), 2.09 (3H, s, $COCH_3$), 2.05−2.00 (1H, m, 2′-H_α), 1.87 (3H, s, CH_3), 0.55 (9H, s, TBDMS), −0.01 (3H, s, TBDMS), −0.37 (3H, s, TBDMS). $^{13}C\{^1H\}$ NMR (DMSO-d_6, 125 MHz): δ 169.3 (1C, $COCH_3$), 163.8 (1C, C-4), 158.0 (2C, DMTr), 150.5 (1C, C-2), 145.0 (1C, DMTr), 136.8 (1C, C-6), 136.0 (1C, DMTr), 135.4 (1C, DMTr), 129.5 (2C, DMTr), 129.4 (2C, DMTr), 127.7 (2C, DMTr), 127.5 (2C, DMTr), 126.4 (1C, DMTr), 113.1 (4C, 1C C-5 and 3C DMTr), 109.7 (1C, DMTr), 84.9 (1C, DMT), 82.3 (1C, 6′-C), 82.2 (1C, 1′-C), 76.9 (1C, 4′-C), 70.1 (1C, 5′-C), 66.0 (1C, 3′-C), 64.1 (1C, 7′-C), 55.0 (2C, 2 ×OCH_3), 36.1 (1C, 2′-C), 25.3 (3C, TBDMS), 17.3 (1C, TBDMS), 12.1 (1C, $COCH_3$), 12.1 (1C, CH_3), −4.7 (1C, TBDMS), −5.8 (1C, TBDMS). HRMS (m/z): $[M + Na]^+$ calcd for $C_{41}H_{52}N_2O_{10}SiNa$, 783.3283; found, 783.3262.

(1*R*)-[(3*S*,4*S*,5*S*,6*R*)-2-Deoxy-5-*O*-[(2-cyanoethyl)-(*N*,*N*-diisopropyl)]phosphoramidite-4-acetyl-3-*O*-*tert*-butyldimethylsilyl-7-*O*-(4,4′-dimethoxytrityl)-β-oxepanyl]thymine (P_1). To a solution of **8** (100 mg, 0.129 mmol) in dry CH_2Cl_2 (1 mL) were added $(^iPr)_2NEt$ (70.0 μL, 0.39 mmol) and 2-cyanoethyl *N*,*N*-diisopropylchlorophosphoramidite (87 μL, 0.39 mmol) at room temperature. The reaction mixture was stirred at 90 °C for 2 h in a microwave sealed reactor vessel tube. CH_2Cl_2 (20 mL) and 5% aq $NaHCO_3$ solution (20 mL) were added, and the resulting mixture was extracted with ethyl acetate. The combined organic layers were dried over anhydrous Na_2SO_4, filtered, and rotaevaporated under reduced pressure. The material left was purified by flash column chromatography on silica gel using a solution of hexane/EtOAc (3:1, v/v) as the eluent. Phosphoramidite **P_1** (116 mg, 0.121 mmol, 94%) was isolated as a white solid. R_f = 0.44, hexane/EtOAc (3:2, v/v). ^{31}P NMR (DMSO-d_6, 81 MHz): δ 151.1, 148.7. HRMS (m/z): $[M + Cl]^-$ calcd for $C_{50}H_{69}N_4O_{11}PSiCl$, 995.4163; found, 995.4151.

(1*R*)-[(3*S*,4*S*,5*S*,6*R*)-2-Deoxy-4-*O*-[(2-cyanoethyl)-(*N*,*N*-diisopropyl)]phosphoramidite-3-acetyl-5-*O*-*tert*-butyldimethylsilyl-7-*O*-(4,4′-dimethoxytrityl)-β-oxepanyl]thymine (P_2). To a solution of **13** (130 mg, 0.17 mmol) in dry CH_2Cl_2 (1 mL) were added $(^iPr)_2NEt$ (92.0 μL, 0.51 mmol) and 2-cyanoethyl *N*,*N*-diisopropylchlorophosphoramidite (114 μL, 0.51 mmol) at room temperature. The reaction mixture was stirred at 90 °C for 2 h in a microwave sealed reactor vessel tube. CH_2Cl_2 (20 mL) and 5% aq $NaHCO_3$ solution (20 mL) were added, and the resulting mixture was extracted with ethyl acetate. The combined organic layers were dried over anhydrous Na_2SO_4, filtered, and rotaevaporated under reduced pressure. The material left was purified by flash column chromatography on silica gel using a solution of hexane/EtOAc (3:1, v/v) as the eluent. Phosphoramidite **P_2** (128 mg, 0.133 mmol, 78%) was isolated as a white solid. R_f = 0.44, hexane/EtOAc (3:2, v/v). ^{31}P NMR (ACN-d_3, 81 MHz): δ 150.3, 150.1. HRMS (m/z): $[M + H]^+$ calcd for $C_{50}H_{70}N_4O_{11}PSi$, 961.4542; found, 961.4560. Small amounts of pure diastereomers were obtained during chromatography; their spectra are shown in the Supporting Information.

(1*R*)-[(3*S*,4*S*,5*S*,6*R*)-2-Deoxy-3-*O*-[(2-cyanoethyl)-(*N*,*N*-diisopropyl)]phosphoramidite-4-acetyl-5-*O*-*tert*-butyldimethylsilyl-7-*O*-(4,4′-dimethoxytrityl)-β-oxepanyl]thymine (P_3). To a solution of **14** (100 mg, 0.13 mmol) in dry CH_2Cl_2 (1 mL) were added $(^iPr)_2NEt$ (35 μL, 0.19 mmol) and 2-cyanoethyl *N*,*N*-diisopropylchlorophosphoramidite (64 μL, 0.19 mmol) at room temperature. The reaction mixture was stirred at this temperature for 15 min. CH_2Cl_2 (20 mL) and 5% aq $NaHCO_3$ solution (20 mL) were added, and the resulting mixture extracted with ethyl acetate. The combined organic layers were dried over anhydrous Na_2SO_4, filtered, and rotaevaporated under reduced pressure. The material left was purified by flash column chromatography on silica gel using a solution of hexane/EtOAc (3:1, v/v) as the eluent. Phosphoramidite **P_3** (97 mg, 0.10 mmol, 78%) was isolated as a white solid. R_f = 0.46, hexane/EtOAc (3:2, v/v). ^{31}P NMR (ACN-d_3, 81 MHz): δ 152.92, 152.79. HRMS (m/z): $[M + Na]^+$ calcd for $C_{50}H_{69}N_4O_{11}PSiNa$, 983.4362; found, 983.4321.

Oligonucleotide Synthesis and Purification. All oligonucleotides (ONs) were synthesized on an Applied Biosystems (ABI) 3400 DNA synthesizer on a 1 μmol scale using UnyLinker CPG as the solid support, mesh 500 Å. DNA phosphoramidites and 2′,4′-modified phosphoramidites were prepared as 0.1 M solutions in acetonitrile and RNA phosphoramidites as 0.15 M solutions in acetonitrile. 5-Ethylthiotetrazole was used as the activator, 3% trichloroacetic acid in dichloromethane was used to deblock DMTr groups, acetic anhydride in tetrahydrofuran (THF) and 16% *N*-methylimidazole in THF were used to cap unreacted 5′-OH groups, and 0.1 M I_2 in 1:2:10 pyridine/water/THF was used for oxidation of phosphite triester linkages. DNA monomers were coupled for 200 s (300 s for dG); all other phosphoramidites were coupled for 600 s (900 s for rG). All oxepane-modified phosphoramidites were coupled for 6000 s. Deprotection and cleavage from the solid support for DNA oligonucleotides were achieved with concentrated aqueous ammonia for 48 h at room temperature. After decanting to remove the CPG, the deprotection solution was removed under vacuum in a SpeedVac lyophilizer. For RNA-containing oligonucleotides, deprotection and cleavage from the solid support were achieved with 3:1 aqueous ammonia/EtOH for 48 h at room temperature, and desilylation was achieved in neat TREAT-HF (150 μL) with shaking at room temperature for 48 h. Purifications were performed by HPLC using a Protein Pak DEAE 5PW analytical anion exchange column. A stationary phase of Milli-Q water and a mobile phase of 1 M $LiClO_4$ in water were used for analysis and purification using a gradient of 0−60% over 37 min. Following purification, excess $LiClO_4$ salts were removed using NAP-25 Sephadex size-exclusion columns. Oligonucleotides were quantitated by UV, and extinction coefficients were determined using the IDT OligoAnalyzer tool (www.idtdna.com/analyzer/Applications/OligoAnalyzer). Extinction coefficients for RNA were used for oligonucleotides containing oxepane modifications.

UV Melting Experiments. Equimolar amounts of complementary sequences were combined, dried, and rediluted in 10 mM sodium phosphate buffer (pH 7.3) containing 140 mM KCl and 1 mM $MgCl_2$ for a final concentration of 1.5 μM for each strand. They were then transferred into cold cuvettes in a UV spectrophotometer. The samples were heated at 75 °C and then cooled to 5 °C at a rate of 0.5 °C/min. The change in absorbance at 260 nm was then monitored upon heating from 5 to 90 °C at a rate of 0.5 °C/min. Each melting experiment was performed three times. Melting temperatures were determined using the hyperchromicity method, and the average and standard deviation values were calculated for each duplex. Thermodynamic parameters were extracted for DNA−RNA duplex (unmodified OxT-modified), as described elsewhere.[32−34]

Circular Dichroism (CD) Spectroscopy. CD spectra were recorded at 5 °C on a JASCO J-810 CD spectrometer equipped with a Peltier temperature controller. Each duplex sample was prepared with 25 μM 5 mM sodium phosphate, 140 mM potassium chloride, 1 mM magnesium chloride buffer, pH 7.3. Each sample was annealed at 90 °C and allowed to cool to room temperature before storing in the fridge overnight. For

https://doi.org/10.1021/acs.joc.1c02254
J. Org. Chem. 2022, 87, 2367−2379

each sample, three scans were accumulated over a wavelength range of 200−320 nm in a 0.1 cm path length cell. Parameters used included a scan rate of 100 nm/min and a response time of 2.0 s. The buffer alone was also scanned, and its spectrum was subtracted from the average scan for each sample. CD spectra were collected in units of millidegrees. Data were smoothed using the Savitzky−Golay function within the JASCO graphing software.

Model Building and Calculations. *Structure Optimization and Force-Field Development.* The structures of the oxepane nucleosides OxT-1, OxT-2, and OxT-3 were energy-optimized at the DFT B3LYP/6-31G* level of theory in Gaussian 16, version B.01.[35] The ESP charges were also calculated at the HF/6-31G* theory. The calculated charges were fitted using the ESP charge fitting protocol.

Duplex Structure Preparation. The structure of the DNA−RNA hybrid was prepared in UCSF chimera[36] using the crystal structure of hybrid with PDB ID: 1G4Q[37] as a template. The DNA duplex was created using the fd_helix routine in NAB in AMBER 18. The oxepane nucleotides were included in the DNA strand to create three modified DNA−RNA hybrid duplexes. In the second stage, the oxepane nucleotides were included in the RNA strand to create three modified RNA−DNA hybrid duplexes. The same sequence of DNA and RNA strands used in the experimental studies were used in the MD studies. The ff99bsc0χ_{OL3}[38,39] force field was used for the RNA strand, and the OL15[40−43] force field was used for the DNA strand. The chiOL4 angle was removed from the OL15 in the case of DNA/RNA hybrids as done by the OL4 developers in the study of HIV-1 Reverse Transcriptase,[44] since it would have minimal effect in the DNA/RNA hybrid duplexes and allow the DNA to adapt better to RNA strand. The TIP3P water model was used, and Na^+ (∼18) ions were added to neutralize the system. The water box was extended to 10 Å from the solute molecules (∼4512 molecules). Three unmodified systems were also prepared as the control for the simulations. A total of 10 systems were studied for 500 ns each.

MD Simulations. Each hybrid-duplex system was subjected to 1000 steps of minimization with 500 steps of steepest descent. Following that, 20 ps of equilibration with a restraint force of 25 kcal/mol/Å^2, at a temperature of 100 K (NVT ensemble) was carried out on the hybrid duplex in the sander. Further 2500 steps of unrestrained minimization with 1000 steps of steepest descent were carried out; 100 ps of unrestrained equilibration using a constant pressure periodic boundary of 1 atm was carried out where the temperature was increased from 100 to 300 K in SANDER. A production run for 500 ns was performed on all of the systems at 300 K using the GPU accelerated version of PMEMD of AMBER 18. The time step used in MD simulations was 2 fs.

MD Simulations Analysis. The CPPTRAJ[45] module of AmberTools was used for the analysis of the simulations. Watson−Crick H-bond distances and occupancies between the O4−N6 and N3−N1 atoms of the bases with a distance cut off of 3.5 Å and an angle cut off of 135. Local base pair parameters like shear, stretch, stagger, propeller, opening, and buckle, local base pair step parameters like tilt, twist, rise, roll, shift, and slide along with the torsion angles, $\alpha, \beta, \gamma, \varepsilon, \zeta, \lambda, \delta$, and κ of the DNA backbone, and the intrastrand phosphate distances were calculated using X3DNA[46] with an ensemble of structures created from the MD. The ensembles of 5000 structures were prepared from the simulation trajectory using CPPTRAJ by taking one structure from every 50 frames of 500 ns. The stacking energy of the systems was calculated using the MINT[47] software package. Ten snapshots captured from every 50 ns of the simulations were considered for the stacking energy calculation. The structures were prepared by stripping off water and ions. The stacking energy was calculated for each base pair, and then the final sum value was for each snapshot was estimated. UCSF Chimera 1.14 and PyMOL 2.3.3 (www.pymol.org) were used for the visualization of trajectory and rendering of images.

■ ASSOCIATED CONTENT

Supporting Information

The Supporting Information is available free of charge at https://pubs.acs.org/doi/10.1021/acs.joc.1c02254.

^{1}H, ^{13}C, ^{31}P, and 2D NMR spectra for compounds **5**−**8**, **10**−**14**, $\mathbf{P_1}$, $\mathbf{P_2}$, and $\mathbf{P_3}$; modeling and dynamics studies (DOCX)

Accession Codes

CCDC 2108264 contains the supplementary crystallographic data for this paper. These data can be obtained free of charge via www.ccdc.cam.ac.uk/data_request/cif, or by emailing data_request@ccdc.cam.ac.uk, or by contacting The Cambridge Crystallographic Data Centre, 12 Union Road, Cambridge CB2 1EZ, UK; fax: +44 1223 336033.

■ AUTHOR INFORMATION

Corresponding Authors

P.I. Pradeepkumar − *Department of Chemistry, Indian Institute of Technology Bombay, Mumbai 400076, India;* orcid.org/0000-0001-9104-3708; Email: pradeep@chem.iitb.ac.in

Masad J. Damha − *Department of Chemistry, McGill University, Montreal, QC H3A 0B8, Canada;* orcid.org/0000-0002-4458-1623; Email: masad.damha@mcgill.ca

Authors

Sunit Kumar Jana − *Department of Chemistry, McGill University, Montreal, QC H3A 0B8, Canada*

S. Harikrishna − *Department of Chemistry, Indian Institute of Technology Bombay, Mumbai 400076, India;* orcid.org/0000-0002-8161-8843

Sruthi Sudhakar − *Department of Chemistry, Indian Institute of Technology Bombay, Mumbai 400076, India*

Roberto El-Khoury − *Department of Chemistry, McGill University, Montreal, QC H3A 0B8, Canada*

Complete contact information is available at: https://pubs.acs.org/10.1021/acs.joc.1c02254

Notes

The authors declare no competing financial interest.

■ ACKNOWLEDGMENTS

We thank the support of the Natural Sciences and Engineering Research Council of Canada (Discovery Grant to M.J.D.) and Ministry of Education-STARS grant and IRCC-IIT Bombay award (to P.I.P.). S.S. thanks the Prime Minister's Research Fellowship (PMRF). This research was enabled in part by support provided by Calcul Québec (www.calculquebec.ca) and Compute Canada (www.computecanada.ca). We acknowledge Prof. Jiří Šponer for suggestions in the molecular dynamics studies.

■ DEDICATION

This paper is dedicated to Prof. Dr. Frank Seela (Osnabrück University) for his important contributions to nucleos(t)ides and nucleic acid chemistry.

■ REFERENCES

(1) Pinheiro, V. B.; Taylor, A. I.; Cozens, C.; Abramov, M.; Renders, M.; Zhang, S.; Chaput, J. C.; Wengel, J.; Peak-Chew, S. Y.; McLaughlin, S. H.; Herdewijn, P.; Holliger, P. Synthetic genetic polymers capable of heredity and evolution. *Science* **2012**, *336*, 341−344.

(2) Yu, H.; Zhang, S.; Chaput, J. C. Darwinan evolution of an alternative genetic system provides support for TNA as an RNA progenitor. *Nat. Chem.* **2012**, *4*, 183−187.

(3) Luo, M.; Groaz, E.; Froeyen, M.; Pezo, V.; Jaziri, F.; Leonczak, P.; Schepers, G.; Rozenski, J.; Marlière, P.; Herdewijn. Invading

Escherichia coli Genetics with a Xenobiotic Nucleic Acid Carrying an Acyclic Phosphonate Backbone (ZNA). *J. Am. Chem. Soc.* **2019**, *141*, 10844−10851.
(4) McKenzie, L. K.; El-Khoury, R.; Thorpe, J. D.; Damha, M. J.; Hollenstein, M. Recent Progress in non-native nucleic acid modifications. *Chem. Soc. Rev.* **2021**, *50*, 5126−5164.
(5) Clercq, E. D. A 40-Year Journey in Search of Selective Antiviral Chemotherapy. *Annu. Rev. Pharmacol. Toxicol.* **2011**, *51*, 1−24.
(6) Herdewijn, P. Nucleic Acids with a Six-Membered 'Carbohydrate' Mimic in the Backbone. *Chem. Biodiversity* **2010**, *7*, 1−59.
(7) Sabatino, D.; Damha, M. J. Oxepane Nucleic Acids: Synthesis, Characterization, and Properties of Oligonucleotides Bearing a Seven-Membered Carbohydrate Ring. *J. Am. Chem. Soc.* **2007**, *129*, 8259−8270.
(8) Habibian, M.; Martínez-Montero, S.; Portella, G.; Chua, Z.; Bohle, D. S.; Orozco, M.; Damha, M. J. Seven-Membered Ring Nucleoside Analogues: Stereoselective Synthesis and Studies on Their Conformational Properties. *Org. Lett.* **2015**, *17*, 5416−5419.
(9) Hoberg, J. O. Formation of Seven-Membered Oxacycles through Ring Expansion of Cyclopropanated Carbohydrates. *J. Org. Chem.* **1997**, *62*, 6615−6618.
(10) Habibian, M.; Harikrishna, S.; Fakhoury, J.; Barton, M.; Ageely, E. A.; Cencic, R.; Fakih, H. H.; Katolik, A.; Takahashi, M.; Rossi, J.; Pelletier, J.; Gagnon, K. T.; Pradeepkumar, P. I.; Damha, M. J. Effect of 2′ −5′ /3′ −5′ phosphodiester linkage heterogeneity on RNA interference. *Nucleic Acid Res.* **2020**, *48*, 4643−4657.
(11) Patrascu, M. B.; Malek-Adamian, E.; Damha, M. J.; Moitessier, N. Accurately Modeling the Conformational Preferences of Nucleosides. *J. Am. Chem. Soc.* **2017**, *139*, 13620−13623.
(12) Malek-Adamian, E.; Patrascu, M. B.; Jana, S. K.; Martínez-Montero, S.; Moitessier, N.; Damha, M. J. Adjusting the Structure of 2′-Modified Nucleosides and Oligonucleotides via C4′-*α*-F or C4′-*α*-OMe Substitution: Synthesis and Conformational Analysis. *J. Org. Chem.* **2018**, *83*, 9839−9849.
(13) O'Reilly, D.; Stein, R. B.; Patrascu, M. B.; Jana, S. K.; Kurian, J.; Moitessier, N.; Damha, M. J. Exploring atypical fluorine-hydrogen bonds and their effects on nucleoside conformations. *Chem.—Eur. J.* **2018**, *24*, 16432−16439.
(14) Clowney, L.; Jain, S. C.; Srinivasan, A. R.; Westbrook, J.; Olson, W. K.; Berman, H. M. Geometric Parameters in Nucleic Acids: Nitrogenous Bases. *J. Am. Chem. Soc.* **1996**, *118*, 509−518.
(15) Tang, X.; Liao, X.; Piccirilli, J. A. 2′-C-Branched Ribonucleosides: Synthesis of the Phosphoramidite derivatives of 2′-C-*β*-Methylcitidine and their incorporation into oligonucleotides. *J. Org. Chem.* **1999**, *64*, 747−754.
(16) Meher, G.; Efthymiou, T.; Stoop, M.; Krishnamurthy, R. Microwave-assisted preparation of nucleoside-phosphoramidites. *Chem. Commun.* **2014**, *50*, 7463−7465.
(17) Damha, M. J.; Usman, N.; Ogilvie, K. K. Solution and solid-phase chemical synthesis of arabinonucleotides. *Can. J. Chem.* **1989**, *67*, 831−839.
(18) Martínez-Montero, S.; Deleavey, G. F.; Martín-Pintado, N.; Fakhoury, J. F.; González, C.; Damha, M. J. Locked 2′-Deoxy-2′,4′-Difluororibo Modified Nucleic Acids: Thermal Stability, Structural Studies, and siRNA Activity. *ACS Chem. Bio.* **2015**, *10*, 2016−2023.
(19) Obika, S.; Nanbu, D.; Hari, Y.; Andoh, J.-i.; Morio, K.-i.; Doi, T.; Imanishi, T. Stability and structural features of the duplexes containing nucleoside analogues with a fixed N-type conformation, 2′-O,4′-C-methyleneribonucleosides. *Tetrahedron Lett.* **1998**, *39*, 5401−5404.
(20) Vanquelef, E.; Simon, S.; Marquant, G.; Garcia, E.; Klimerak, G.; Delepine, J. C.; Cieplak, P.; Dupradeau, F.-Y. RED Server: A Web Service for Deriving RESP and ESP Charges and Building Force Field Libraries for New Molecules and Molecular Fragments. *Nucleic Acids Res.* **2011**, *39* (suppl_2), W511−W517.
(21) Dupradeau, F.-Y.; Pigache, A.; Zaffran, T.; Savineau, C.; Lelong, R.; Grivel, N.; Lelong, D.; Rosanski, W.; Cieplak, P. The REd. Tools: Advances in RESP and ESP Charge Derivation and Force Field Library Building. *Phys. Chem. Chem. Phys.* **2010**, *12* (28), 7821−7839.
(22) Case, D. A.; Ben-Shalom, I. Y.; Brozell, S. R.; Cerutti, D. S.; Cheatham, T. E., III; Cruzeiro, V. W. D.; Darden, T. A.; Duke, R. E.; Ghoreishi, D.; Gilson, M. K. *AMBER 2018*, University of California, San Franciso, 2018.
(23) Götz, A. W.; Williamson, M. J.; Xu, D.; Poole, D.; Le Grand, S.; Walker, R. C. Routine Microsecond Molecular Dynamics Simulations with AMBER on GPUs. 1. Generalized Born. *J. Chem. Theory Comput.* **2012**, *8* (5), 1542−1555.
(24) Salomon-Ferrer, R.; Götz, A. W.; Poole, D.; Le Grand, S.; Walker, R. C. Routine Microsecond Molecular Dynamics Simulations with AMBER on GPUs. 2. Explicit Solvent Particle Mesh Ewald. *J. Chem. Theory Comput.* **2013**, *9* (9), 3878−3888.
(25) Le Grand, S.; Götz, A. W.; Walker, R. C. SPFP: Speed without Compromise - A Mixed Precision Model for GPU Accelerated Molecular Dynamics Simulations. *Comput. Phys. Commun.* **2013**, *184* (2), 374−380.
(26) Galindo-Murillo, R.; Robertson, J. C.; Zgarbová, M.; Šponer, J.; Otyepka, M.; Jurečka, P.; Cheatham, T. E. Assessing the Current State of Amber Force Field Modifications for DNA. *J. Chem. Theory Comput.* **2016**, *12* (8), 4114−4127.
(27) Entrena, A.; Campos, J. M.; Gallo, M. A.; Espinosa, A. Rules for Predicting the Conformational Behavior of Saturated Seven-Membered Heterocycles. *Arkivoc* **2005**, *2005* (6), 88−108.
(28) Entrena, A.; Campos, J.; Gómez, J. A.; Gallo, M. A.; Espinosa, A. A New Systematization of the Conformational Behavior of Seven-Membered Rings. Isoclinal Anomeric and Related Orientations. *J. Org. Chem.* **1997**, *62* (2), 337−349.
(29) Hartmann, B.; Piazzola, D.; Lavery, R. BI - BII Transitions in B-DNA. *Nucleic Acids Res.* **1993**, *21* (3), 561−568.
(30) Migawa, M. T.; Shen, W.; Wan, W. B.; Vasquez, G.; Oestergaard, M. E.; Low, A.; De Hoyos, C. L.; Gupta, R.; Murray, S.; Tanowitz, M.; Bell, M.; Nichols, J. G.; Gaus, H.; Liang, X. H.; Swayze, E. E.; Crooke, S. T.; Seth, P. P. Site-specific replacement of phosphorothioate with alkyl phosphonate linkages enhances the therapeutic profile of gapmer ASOs by modulating interactions with cellular proteins. *Nucleic Acids Res.* **2019**, *47* (11), 5465−5479.
(31) Ageely, E. A.; Chilamkurthy, R.; Jana, S.; Abdullahu, L.; O'Reilly, D.; Jensik, P. J.; Damha, M. J.; Gagnon, K. T. Gene editing with CRISPR-Cas12a guides possessing ribose-modified pseudoknot handles. *Nat Commun* **2021**, *12*, 6591−6606.
(32) Mergny, J.-L.; Lacroix, L. Analysis of thermal melting curves. *Oligonucleotides* **2003**, *13*, 515−537.
(33) Jana, S. K.; Leonard, P.; Ingale, S. A.; Seela, F. 2′-*O*-Methyl- and 2′-*O*-propargyl-5-methylisocytidine: synthesis, properties and impact on the isoC$_d$-dG and the isoC$_d$-isoG$_d$ base pairing in nucleic acids with parallel and antiparallel strand orientation. *Org. Biomol. Chem.* **2016**, *14*, 4927−4941.
(34) Jana, S. K.; Guo, X.; Mei, H.; Seela, F. Robust silver-mediated imidazolo-dC base pairs in metal DNA: dinuclear silver bridges with exceptional stability in double helices with parallel and antiparallel strand orientation. *Chem. Commun.* **2015**, *51*, 17301−17304.
(35) Frisch, M. J.; Trucks, G. W.; Schlegel, H. B.; Scuseria, G. E.; Robb, M. A.; Cheeseman, J. R.; Scalmani, G.; Barone, V.; Petersson, G. A.; Nakatsuji, H. *Gaussian 16*, revision B.01; Gaussian, Inc.: Wallingford, CT, 2016.
(36) Pettersen, E. F.; Goddard, T. D.; Huang, C. C.; Couch, G. S.; Greenblatt, D. M.; Meng, E. C.; Ferrin, T. E. UCSF Chimera - A Visualization System for Exploratory Research and Analysis. *J. Comput. Chem.* **2004**, *25* (13), 1605−1612.
(37) Han, G. W. Direct-Methods Determination of an RNA/DNA Hybrid Decamer at 1.15 Å Resolution. *Acta Crystallogr. Sect. D Biol. Crystallogr.* **2001**, *57* (2), 213−218.
(38) Banáš, P.; Hollas, D.; Zgarbová, M.; Jurečka, P.; Orozco, M.; Cheatham, T. E.; Šponer, J.; Otyepka, M. Performance of Molecular Mechanics Force Fields for RNA Simulations: Stability of UUCG and GNRA Hairpins. *J. Chem. Theory Comput.* **2010**, *6* (12), 3836−3849.
(39) Zgarbová, M.; Otyepka, M.; Šponer, J.; Mládek, A.; Banáš, P.; Cheatham, T. E.; Jurečka, P. Refinement of the Cornell et Al. Nucleic Acids Force Field Based on Reference Quantum Chemical Calculations

https://doi.org/10.1021/acs.joc.1c02254
J. Org. Chem. 2022, 87, 2367−2379

of Glycosidic Torsion Profiles. *J. Chem. Theory Comput.* **2011**, *7* (9), 2886−2902.
(40) Zgarbová, M.; Šponer, J.; Otyepka, M.; Cheatham, T. E.; Galindo-Murillo, R.; Jurečka, P. Refinement of the Sugar-Phosphate Backbone Torsion Beta for AMBER Force Fields Improves the Description of Z- and B-DNA. *J. Chem. Theory Comput.* **2015**, *11* (12), 5723−5736.
(41) Wang, J.; Cieplak, P.; Kollman, P. A. How Well Does a Restrained Electrostatic Potential (RESP) Model Perform in Calculating Conformational Energies of Organic and Biological Molecules? *J. Comput. Chem.* **2000**, *21* (12), 1049−1074.
(42) Pérez, A.; Marchán, I.; Svozil, D.; Sponer, J.; Cheatham, T. E.; Laughton, C. A.; Orozco, M. Refinement of the AMBER Force Field for Nucleic Acids: Improving the Description of α/γ Conformers. *Biophys. J.* **2007**, *92* (11), 3817−3829.
(43) Bayly, C. I.; Merz, K. M.; Ferguson, D. M.; Cornell, W. D.; Fox, T.; Caldwell, J. W.; Kollman, P. A.; Cieplak, P.; Gould, I. R.; Spellmeyer, D. C. A Second Generation Force Field for the Simulation of Proteins, Nucleic Acids, and Organic Molecules. *J. Am. Chem. Soc.* **1995**, *117* (19), 5179−5197.
(44) Figiel, M.; Krepl, M.; Poznański, J.; Gołab, A.; Šponer, J.; Nowotny, M. Coordination between the Polymerase and RNase H Activity of HIV-1 Reverse Transcriptase. *Nucleic Acids Res.* **2017**, *45* (6), 3341−3352.
(45) Roe, D. R.; Cheatham, T. E. PTRAJ and CPPTRAJ: Software for Processing and Analysis of Molecular Dynamics Trajectory Data. *J. Chem. Theory Comput.* **2013**, *9* (7), 3084−3095.
(46) Lu, X.-J.; Olson, W. K. 3DNA: A Versatile, Integrated Software System for the Analysis, Rebuilding and Visualization of Three-Dimensional Nucleic-Acid Structures. *Nat. Protoc.* **2008**, *3* (7), 1213.
(47) Górska, A.; Jasiński, M.; Trylska, J. MINT: Software to Identify Motifs and Short-Range Interactions in Trajectories of Nucleic Acids. *Nucleic Acids Res.* **2015**, *43* (17), No. e114.

https://doi.org/10.1021/acs.joc.1c02254
J. Org. Chem. 2022, 87, 2367−2379